# Optimized imaging of the midface and orbits

## Abstract

A variety of imaging techniques are available for imaging the midface and orbits. This review article describes the different imaging techniques based on the recent literature and discusses their impact on clinical routine imaging. Imaging protocols are presented for different diseases and the different imaging modalities.

Keywords: imaging, midface, orbits, CT, MRI

Sönke Langner[1]

1 Institute for Diagnostic Radiology and Neuroradiology, University Medicine Greifswald, Germany

## 1 Introduction

The complex anatomy of the nose, the paranasal sinuses, the orbits, and the adjacent anatomical compartments of the neck poses a diagnostic challenge for both clinical examinations and diagnostic imaging.

Traumatic lesions usually present with unique clinical features, and high-resolution imaging is needed to precisely describe their anatomical location and extent [1], [2]. On the other hand, clinical signs of tumors of the midface are often unspecific [3], [4]. Therefore, most patients have advanced disease at the time of diagnosis [4]. In tumor patients, imaging is needed to precisely evaluate the local tumor extent, especially if the area is not accessible clinically, and to identify lymphatic involvement and distant metastases. In oncologic patients, imaging is needed to monitor the treatment response and to differentiate between residual and recurrent tumor or treatment-related changes [4].

This review will present the different imaging modalities for sinonasal and orbital imaging, and their clinical relevance will be discussed with respect to the recent literature. Imaging protocols for the different modalities and disease entities will be provided.

## 2 Conventional radiography (CR)

Conventional radiography is a projection technique generating a two-dimensional (2D) image. The increasing availability of flat panel detectors for image detection has significantly decreased radiation exposure [5], because flat panel detectors are more sensitive to radiation and provide better image quality with less radiation exposure [6].

Because the different structures are projected onto each other, conventional radiographs (CR) are of limited diagnostic value (Figure 1) for assessment of the paranasal sinuses and have become obsolete in the diagnosis of acute or chronic rhinosinusitis. They are therefore not recommended by the major societies [7], [8]. In a pro-spective study of 134 patients who underwent CR and computed tomography (CT) examinations of the paranasal sinuses on the same day, Konen et al. found CR to be inferior to CT in diagnostic accuracy [9]. The sensitivity of CR for the detection of inflammatory changes of the maxillary sinus was 67.7%, but only 14.6% and 3.8% for the ethmoid and sphenoid sinus, respectively, compared to low-dose CT (ldCT) (Figure 1).

Because soft tissue changes are only poorly visualized, CR plays no role in tumor imaging [8].

Kim et al., in a retrospective study of 92 patients, found a sensitivity of 85.7% and 88.7% sensitivity for the detection of fractures of the orbital floor or the lamina pap-yracea in comparison to CT [10]. The authors claim that fractures that were missed by CR did not need surgical treatment; however, they do not provide any details on functional outcome in the patients with missed fractures on CR. Furthermore, herniation of orbital content cannot be appreciated accurately on CR. Therefore, a CT should be obtained when a facial fracture is suspected clinically (Figure 2) [1], [8], [11], [12].

## 3 Digital volume tomography (DVT)

Digital volume tomography (DVT) or "cone beam tomography" is a recent technical development based on the principle of orthopantomography. As with CT, the X-ray beam in DVT rotates around the patient but is conical in configuration, while it is fan-shaped in CT [13]. During a rotation, which may cover 180° or 360°, multiple 2D X-ray images are recorded, which are then assembled into a three-dimensional (3D) volume dataset by the application software [13]. This dataset can then be reviewed in any plane (Figure 3) or be further processed three-dimensionally.

DVT systems for clinical use have been available since 1982. With their wider availability, they are increasingly being used for different ear, nose, and throat (ENT) applications [8], [14].

**Figure 1: 53-year-old patient with leukemia prior to radiation therapy.**
a) Conventional radiograph of the paranasal sinuses; soft tissue swelling within the right maxillary sinus without air-fluid level.
b) CT of the paranasal sinuses of the same patient. The CT was performed 2 hours after plain radiographs. CT shows sinusitis of the sphenoid sinus not detectable on the radiographs.
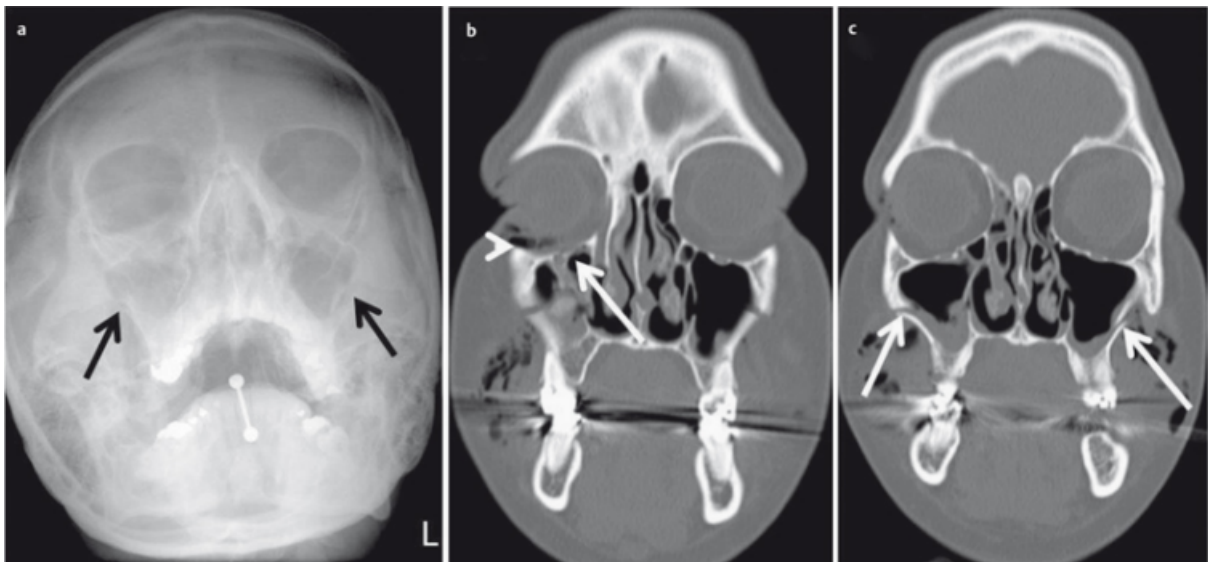c) CT does not confirm sinusitis of the right maxillary sinus.



**Figure 2: 22-year-old drunken patient having received blows to the face.**
a) Conventional radiography of the paranasal sinuses. Suboptimal image quality due to lack of compliance. There is a fracture of the lateral aspects of both maxillary sinuses (arrow), additional fractures are not detectable.
b) CT of the midface, coronal plane; fracture of the floor of the orbit (arrow) and intraorbital air (arrowhead).
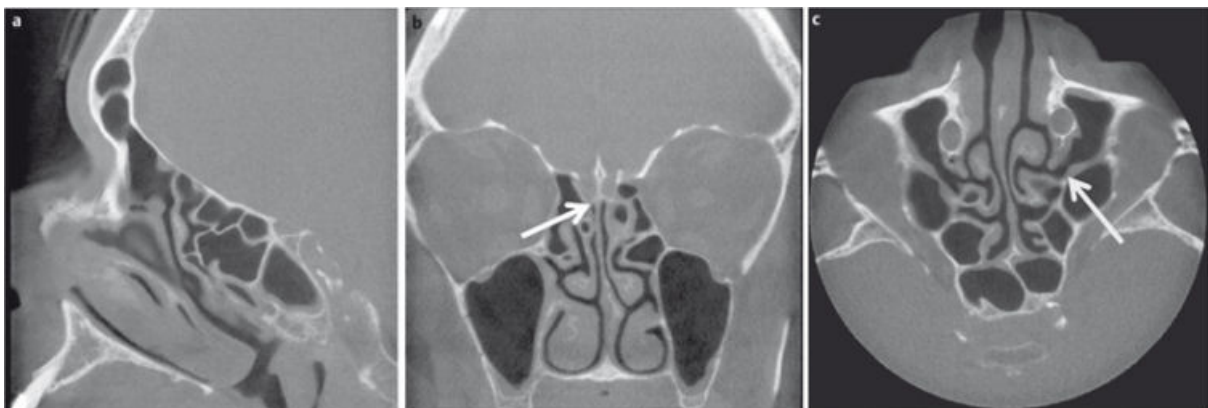c) CT of the midface allows precise determination of the extent of the fracture (arrow).



**Figure 3: DVT of a 43-year-old patient with clinically suspected exacerbation of chronic rhinosinusitis.**
a) Sagittal plane at the level of the fronto-ethmoid recess (arrow).
b) Coronal plane at the level of the cribriform plate (arrow).
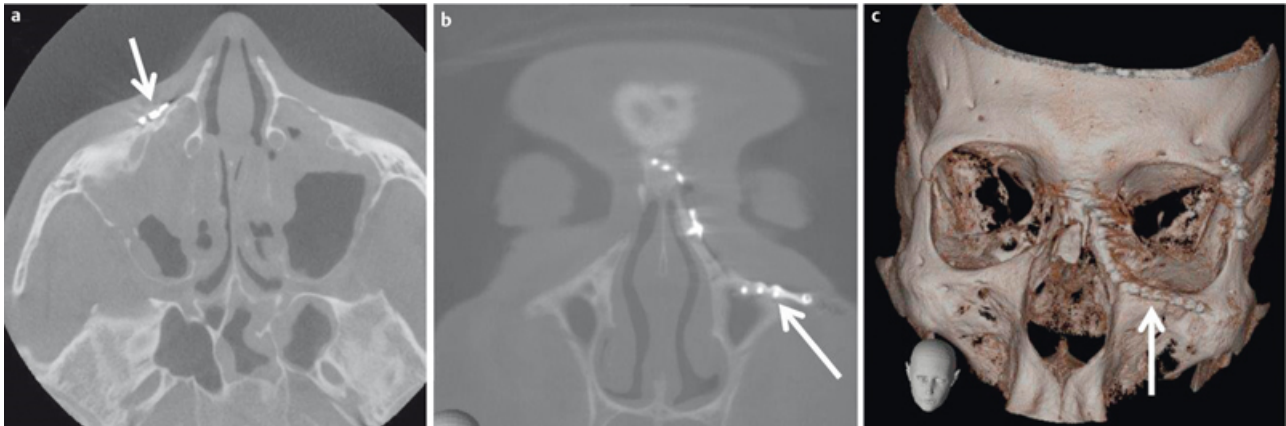c) Axial plane at the level of the ostiomeatal complex (arrow).

**Figure 4: DVT of 19-year-old patient after surgery for a complex fracture of the midface.**
a) Axial plane; only discrete artifacts caused by the osteosynthetic material (arrow).
b) Coronal plane demonstrating the position of the small plate (arrow).
c) 3D VRT reconstruction (volume rendering technique, VRT) confirming correct placement of the implants.
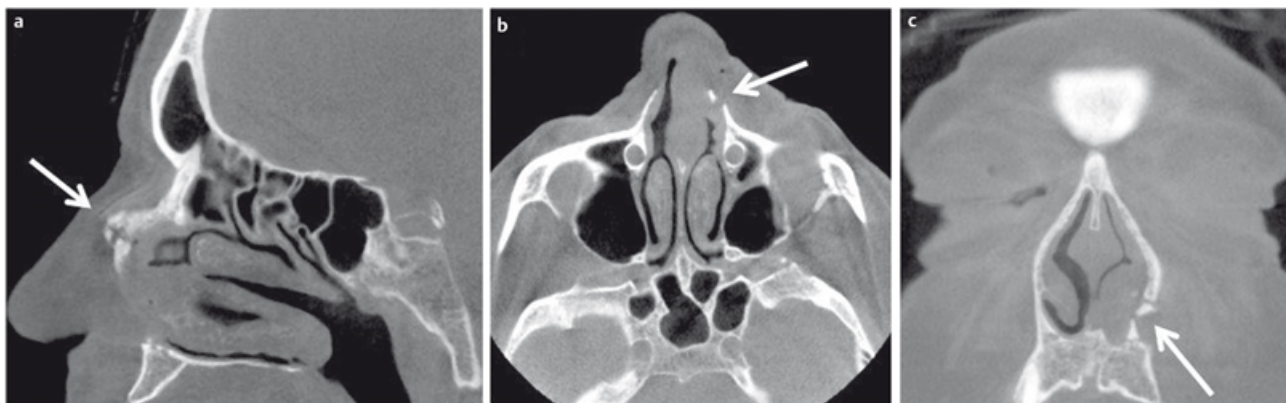


**Figure 5: 83-year-old female patient who fell due to cardiac event.** DVT allows identification of the precise anatomical location of the fragment of the nasal fracture in all planes (a = sagittal, b = axial, c = coronal).

DVT systems produce images with a highly isotropic (i.e., the dimension of the volume pixel, or voxel, is the same in all three spatial directions) local resolution at relatively low radiation exposure [14], [15], [16]. With the radiation dose used and the postprocessing algorithms available, DVT allows the delineation of fine bony structures [17] and is less sensitive to artifacts of metal dental implants (Figure 4) than CT [18]. Various commercial DVT systems are available for clinical routine imaging with the patient in different positions (standing, sitting, or lying). Unlike CT, the volume of interest (VOI) has to be defined in DVT prior to image acquisition. This VOI depends on the indication for imaging [18] and should include a cylinder of 10×10 cm when imaging the paranasal sinuses. For imaging the nasal skeleton, a cylinder of 4×4 cm is considered sufficient.

With its excellent spatial resolution, DVT is considered a valid alternative to CT in the diagnosis of fractures. Because DVT systems were initially used for imaging of dental fractures [14], comprehensive scientific data are available. However, there is also an increasing number of publications on the use of DVT in imaging facial fractures [19]. In a prospective patient population, Choudhary et al. [20] demonstrated the superiority of DVT over conventional radiography for the detection of midfacial fractures. However, in the acute trauma setting, DVT is rarely used because positioning of the patient in the DVT system is not possible and CT continues to be the preferred imaging modality [17], [21].

In a prospective collective of 65 patients, Bremke et al. found DVT to be superior to CR in the detection of nasal fractures [19]. While only 5 fractures were missed on CR, exact spatial mapping of the fracture and of the dislocated fragments was improved using DVT (Figure 5). DVT is also suitable for postoperative imaging after osteosynthetic treatment of facial fractures because it is less sensitive to metal artifacts than CT (Figure 4). DVT datasets can also be used for neuronavigation with some clinical neuronavigation systems. However, in these cases, a large VOI is required (Figure 6).

Another important application of DVT is imaging of the paranasal sinuses (Figure 7) in patients with chronic rhinosinusitis [14], [16], [18], [22]. Leiva-Salinas et al. [15] prospectively evaluated 40 patients with inflammatory changes of the paranasal sinuses who underwent paranasal DVT and CT within 1 hour. Although image quality of DVT was inferior to that of CT, this did not affect diagnostic accuracy while significantly decreasing radiation exposure. This is of particular importance because the majority of patients with rhinosinusitis are young

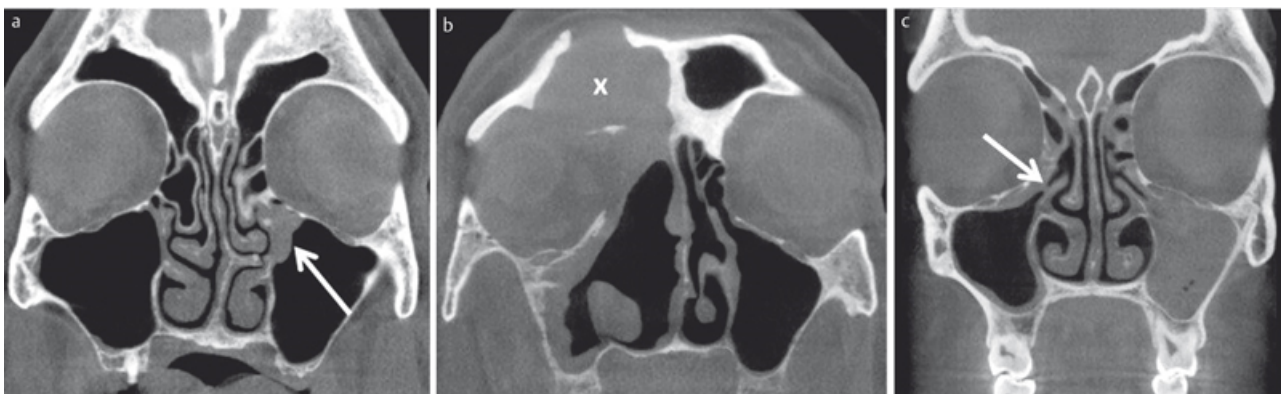Figure 6: Neuronavigation (brainlab®) using a DVT dataset.



**Figure 7: DVT images in coronal plane in different patients with inflammatory changes of the paranasal sinuses.**
a) 56-year-old female patient with chronic rhinosinusitis presenting with new onset of pain and feeling of pressure in the left maxillary sinus. Obstruction of the ostiomeatal complex (arrow).
b) 72-year-old patient with chronic sinusitis and multiple surgical treatments. Exacerbation and new onset of pain in the right maxillary sinus. DVT demonstrates inflammatory tissue swelling. The mucocele of the frontal sinus was asymptomatic.
c) 22-year-old female patient with recurrent rhinosinusitis and bilateral facial pain. Complete opacification of the left maxillary sinus and obstruction of right ostiomeatal complex.

adults [15], in whom reduction of radiation exposure is a crucial concern [23], [24], especially if repeated imaging is needed in chronic disease [25]. In these cases, magnetic resonance imaging (MRI) has to be considered as an alternative imaging modality [8].

Radiation exposure is higher for a conventional CT scan of the paranasal sinuses compared to a DVT study [15].
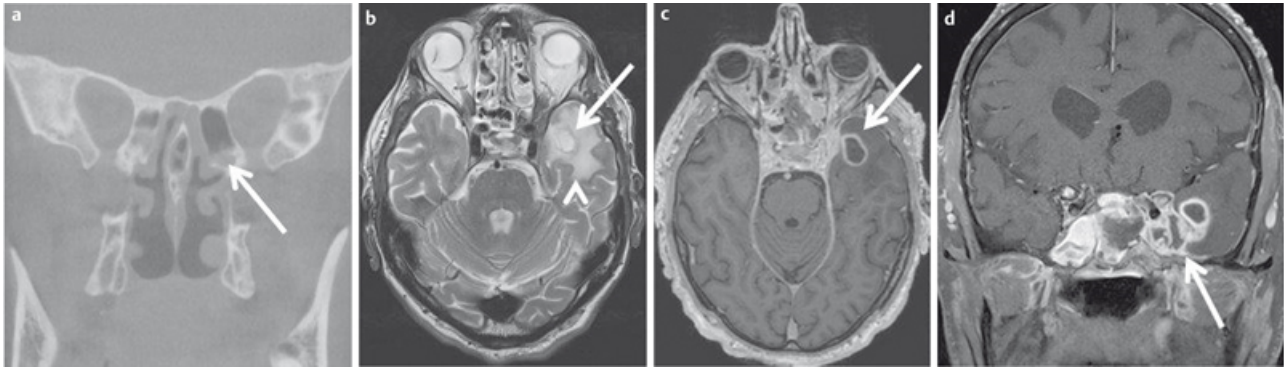
**Figure 8: 67-year-old diabetic patient with numb centrally located headache.**
a) Coronal reconstructed DVT demonstrates inflammatory changes of the posterior ethmoid cells (arrow) and the sphenoid sinus on the left side.
b) New onset of seizure a few hours after the DVT. T2w MR images demonstrate a ring-like mass (arrow) with surrounding edema (arrowhead).
c) The lesion displays homogenous ring-like enhancement on axial T1w images.
d) Contrast-enhanced coronal T1w images demonstrate extension to the dura and the thrombosed cavernous sinus. Fungal sinusitis was confirmed by surgery.

However, DVT systems have a wide range of effective doses applied to the patient as demonstrated in a study by Rottke et al. [16], who evaluated 10 different DVT systems. These results were reproduced by other authors. Therefore, these investigators recommend optimization and critical review of the default DVT study protocols provided by manufacturers [15], [16], [26].

For technical reasons, DVT provides inferior soft tissue contrast. Therefore, DVT plays only a minor role in the diagnosis of facial tumors and is inferior to CT and MRI in detecting complications of sinusitis (Figure 8). Fakhran et al. [22] analyzed how many soft tissue processes are missed by DVT examinations. In their retrospective study of 361 patients included over a period of one year, they generated virtual DVT datasets from conventional CT examinations of the midface. The authors rated any soft tissue process that was not located on a border with an air-filled structure as not detected by DVT. They were able to show that, with this approach, less than 3.5% of patients had a lesion that would have been missed by DVT. Additionally, these potentially missed lesions were already known in 2/3 of the patients. These results indicate that appropriate patient selection is of high clinical relevance. In immunocompromised patients or in patients with suspected invasive fungal sinusitis or with orbital or intracranial complications, CT should be performed [22].

The use of contrast agents in DVT examinations to improve soft tissue contrast is still experimental [27]. Alsufyani et al. showed that the mucosal surface of the paranasal sinuses is best opacified by using 25% barium sulfate, while iodine-containing contrast agents are not suitable [28]. However, even with this approach, the authors failed to reliably opacify soft tissues cranial to the middle turbinate [28].

Studies comparing DVT and CT are still limited. The current guidelines list DVT as a possible alternative for head and neck imaging [7], [21], [29] but make no specific recommendations [8].

# 4 Computed tomography (CT)

Computed tomography (CT) is the most commonly used modality for head and neck imaging [7], [8]. Major advantages of CT are the availability and the short examination time, which is well tolerated by the majority of patients. Another, increasingly more important aspect are the costs in comparison to MRI [30].

For a CT examination, the patient lies on a table with the tube rotating around the patient. In contrast to DVT, the X-ray beam is fan-shaped. Opposite to the tube is the detector, which registers beam attenuation and converts it into a grayscale image. The grayscale of each voxel can be quantified in Hounsfield units, which are used to characterize different tissues [31].

The different grayscale values which can be differentiated by the eye have to be allocated to a specific range of Hounsfield units, the so-called "window-level-setting", to improve image contrast. Different window-level settings are available, from which the radiologist must choose the best one for a given clinical question to be answered (Figure 9).

The multidetector CT (MDCT) scanners available in clinical routine yield high-resolution axial volume datasets with submillimeter spatial resolution [32]. Images in different planes can be reconstructed secondarily from these datasets without the need for additional radiation exposure or a loss of image information [33]. Primary coronary CT scans of the paranasal sinuses have become obsolete [34] because artifacts caused by metal dental implants are significantly enhanced (Figure 10) compared to axial scans [34], [35]. Tumor imaging cannot be performed without IV administration of an iodine-based contrast agent. These contrast agents are hypo- or iso-osmolar to serum and have a low profile for adverse events [36].
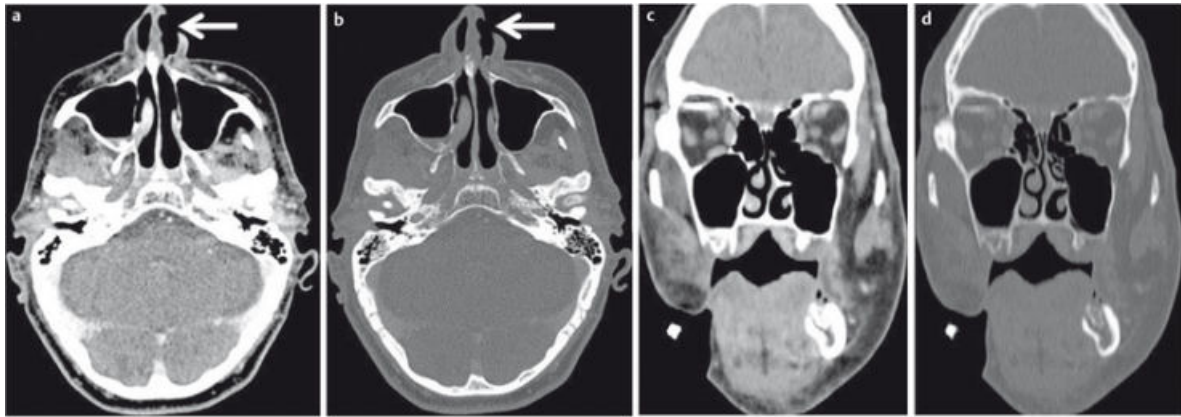
**Figure 9: 67-year-old patient after surgical treatment of a malignant melanoma of the left nose.** CT of the midface in axial (a,b) and coronal (c,d) planes with different window-level settings (soft tissue window level: a,c; bone window level: b,d). The window-level setting has to be chosen according to the tissue to be evaluated.
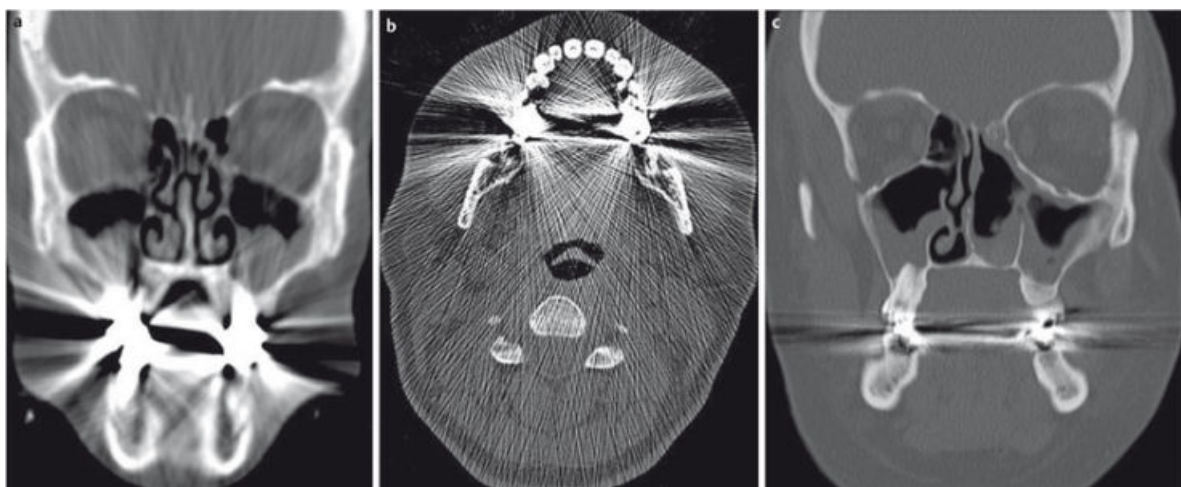


**Figure 10: The occurrence of artifacts depends on the primary acquisition plane of the CT.**
a) 32-year-old female patient; CT of the paranasal sinuses acquired in primary coronal plane. Reduced image quality and diagnostic accuracy due to severe artifacts.
b) 37-year-old patient with chronic rhinosinusits. CT acquired in primary axial plane is degraded by severe artifacts due to dental implants.
c) Secondary reconstructed coronal plane of the same patient as in b. The artifacts are limited to the acquisition plane. Therefore, image quality and diagnostic accuracy of the paranasal sinuses are not reduced.

## 4.1 Fractures of the midface

Midface injuries occur in approximately 25% of all trauma patients [37]. In addition to the clinical examination, imaging is crucial for the management of these patients. The imaging modality of choice is CT [38] because the midfacial CT scan is usually part of the routine trauma CT scan or can be performed immediately afterwards [39]. Planning of surgery is often facilitated by 3D preoperative planning (Figure 11, Figure 12) [37].

## 4.2 Imaging of paranasal sinuses

Sinusitis is the most common disease of the paranasal sinuses and has both a clinical and a socioeconomic impact. Acute sinusitis is a clinical diagnosis and imaging is not required routinely. In chronic sinusitis, however, imaging is needed for treatment planning.

When imaging high-contrast structures such as the paranasal sinuses, higher image noise is acceptable. Therefore radiation exposure can be reduced [40] without a relevant loss of image quality or decrease in diagnostic accuracy. With the use of these so-called low-dose CT (ldCT) protocols it is possible to image the paranasal sinuses with radiation exposure similar to conventional radiographs and DVT [3], [25]. Therefore, ldCT is the imaging technique of choice in the diagnostic work-up of chronic sinusitis [7], [8], [18]. Compared to DVT, ldCT also provides an excellent display of the anatomy and the anatomical variants of the paranasal sinuses (Figure 13) before Functional Endoscopic Sinus Surgery (FESS) [41]. In a phantom study, Kröpil et al. [42] demonstrated that radiation exposure of ldCT can be further reduced by the use of special post-processing filters. However, this technique needs processing steps. In another phantom study, Schulz et al. demonstrated that similar effects can be achieved by using a special image
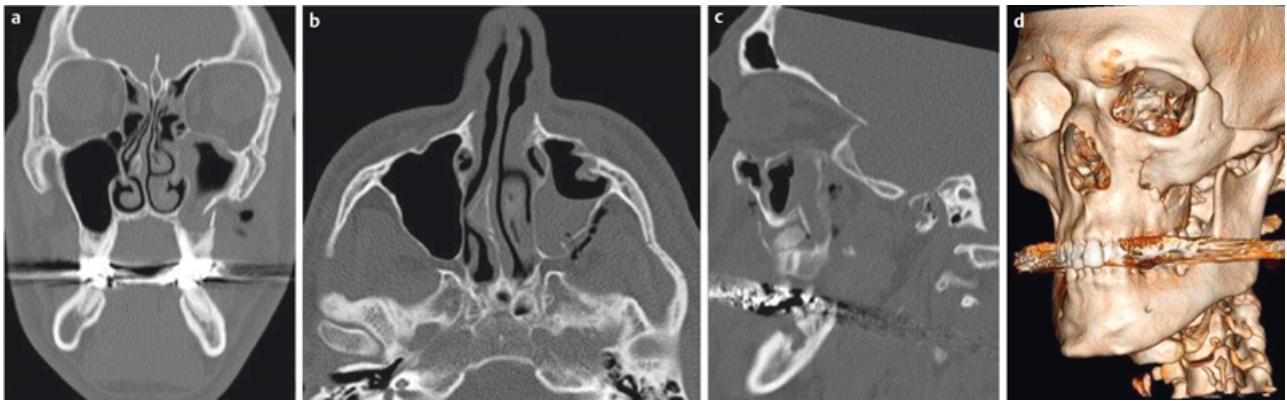
**Figure 11: 19-year-old patient who fell on the face.** CT of the midface in bone window-level setting (a–c) demonstrates the exact extent of the complex fracture of the maxillary sinus, zygomatic arch ("tripod fracture"), and the floor of the orbit. 3D-VRT reconstruction demonstrates the anatomical relationship of the different fragments.
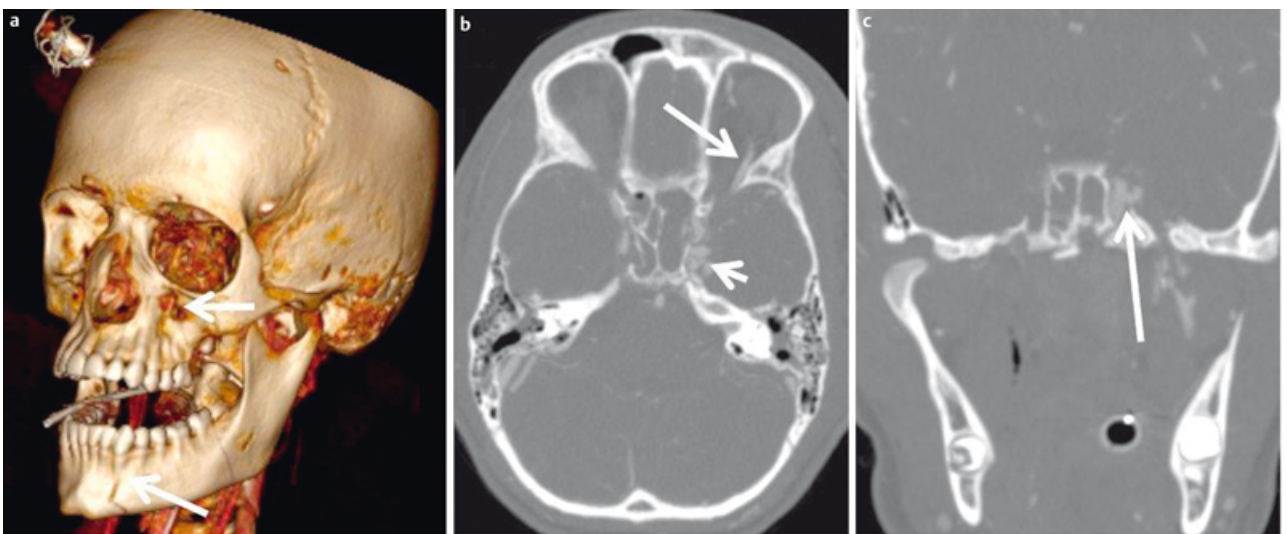


**Figure 12: 16-year-old patient with severe trauma to the head and progressive exophthalmos and chemosis.**
a) 3D-VRT reconstruction demonstrates the extent of the fracture with only minimal displacement of the fragments.
b) Contrast-enhanced CT angiography demonstrates opacification of the cavernous sinus (short arrow) and the superior ophthalmic vein (long arrow) indicating carotid cavernous sinus fistula.
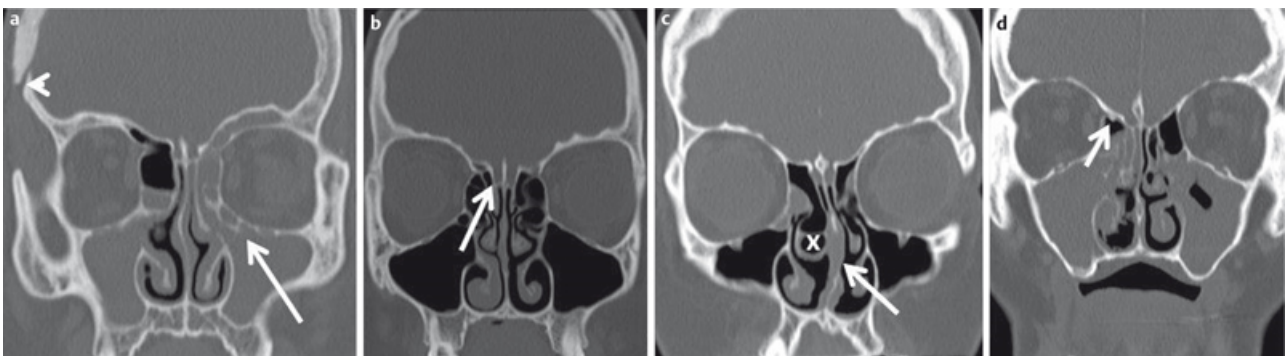c) Coronal MIP reconstruction (maximum intensity projection, MIP) demonstrates the fistula (arrow).



**Figure 13: Relevant anatomical variants of the paranasal sinuses prior to FESS.**
a) 43-year-old patient with chronic rhinosinusitis and recurrent surgery; complete opacification of the maxillary sinus on both sides. Haller cell (arrow) on the left side causing obstruction of the left ostiomeatal complex along with an ethmoid bulla. The patient underwent cranial surgery (arrowhead) due to meningioma.
b) 19-year-old female patient; ethmoid bulla on the left side. Keros type II Cribriform plate variant.
c) 37-year-old patient prior to surgery. Concha bullosa of the middle turbinate on the right side (x). Left convex deviation of the nasal septum (arrow) with small bony spur. Small Haller cell and opacified ethmoid bulla on the right side.
d) 56-year-old patient with exacerbation of chronic rhinosinusitis after repeated surgery. Small bony spur in the course of the anterior ethmoid artery (arrow). Keros type I cribriform plate variant.
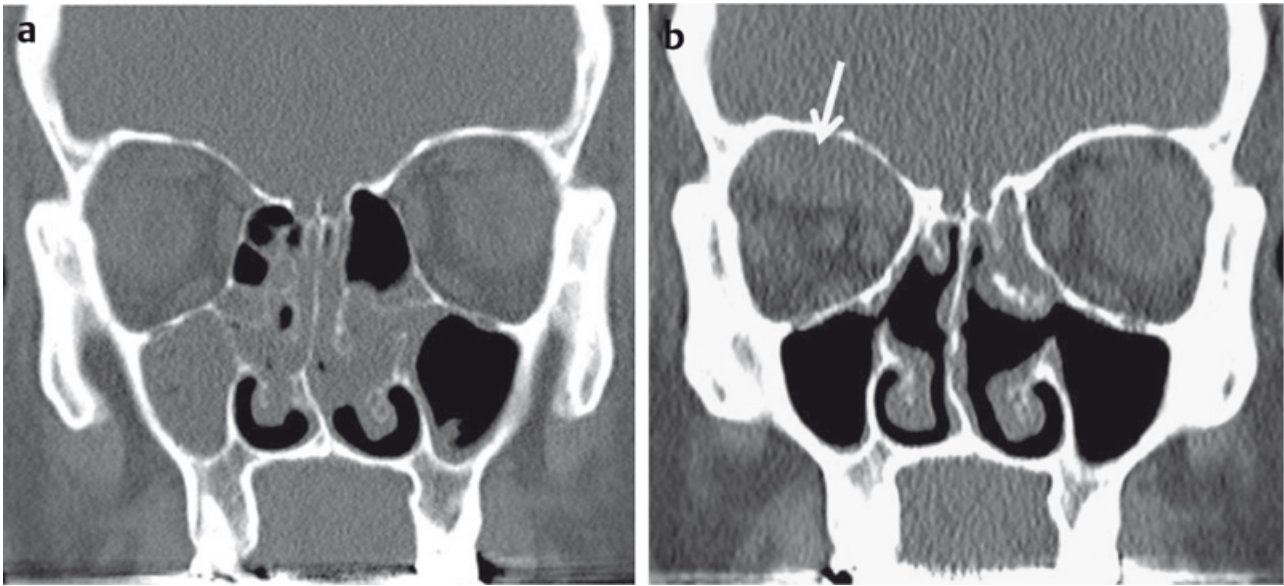
**Figure 14: 63-year-old diabetic patient with exacerbation of chronic rhinosinusitis.**
a) CT of the paranasal sinuses, coronal reconstructed image in bone window-level setting. Complete opacification of the right maxillary sinus and obstructed left ostiomeatal complex.
b) Follow-up CT two weeks later after conservative therapy. New onset of headache and diplopia. Coronal reconstructed image in bone window-level setting demonstrates a smoothly marginated subperiostal lesion. Abscess formation was confirmed by surgery.

reconstruction technique, so-called iterative reconstruction [43]. These experimental findings were confirmed by Bulla et al. in a feasibility study of 80 patients [44]. By using iterative methods of reconstruction they could reduce the dose of an ldCT protocol by 68% compared to a standard CT protocol. In contrast to DVT, the dose reductions that can be achieved are similar for different CT scanners. Therefore, CT examinations have a significantly lower variation in radiation exposure compared to DVT, as also demonstrated in a prospective study of Hoxworth et al. [45].

CT is also the imaging technique of choice when complications of sinusitis are suspected (Figure 14). However, in these patients, standard CT protocols should be used instead of ldCT and administration of contrast agent is mandatory [8], [46], [47]. However, CT is inferior to MRI for the detection of intracranial complications (Figure 15) [46], [47].

When imaging the midface, the eye lens – the most radiation-sensitive part of the body – lies within the beam [48]. The threshold for cataract induction specified in the literature is 0.5–2 Sievert (Sv) [49]. For fractional repeated radiation exposure, a threshold of 0.1 SV has been reported [50]. In a population-based retrospective evaluation of 2,276 patient and 27,761 controls, Yuan et al. calculated a *hazard ratio* of up to 2.12 and a percentage increase of up to 1.45% for cataract induction after repeated CT studies of the head and neck [51]. Although this is the study with the largest number of patients, its results are discussed controversially. One of the main criticisms is that the patient group consisted of cancer patients and the impact of concomitant chemotherapy was not taken into account [52]. A reduction of lens radiation can, in addition to modification of the scanning protocol or image reconstruction, further be achieved by a special lens cap (Figure 16), which is worn like a pair of glasses [53]. In a phantom study, Keil et al. calculated a dose reduction for the lens with the use of such lens protection devices that ranged from 38–48%, depending on the material used [54]. The latest-generation CT scanners offer organ-related tube current modulation (TCM) [55], [56], [57]. Wang et al. showed, in a phantom study, that the synergistic effect of TCM and lens protection results in a significant reduction of 47% of the lens dose [58]. Plessow et al. [59] validated these results in a prospective study of patients examined on a latest-generation CT scanner. Their results show that lens protection devices and ldCT protocols can be used without a loss of diagnostic accuracy (Figure 17).

## 4.3 Tumors of the midface

Tumors of the midface are rare and account for approximately 3% of all head and neck malignancies [60], [61]. Men are more often affected, and the peak age is between 50 and 70 years. CT is the imaging method of choice due to its availability and the short examination times. However, MRI is superior for the detection of submucosal or perineural tumor spread (see MRI section). In comparison CT is superior to MRI for the detection if osseous infiltration of small bony structures is suspected (Figure 18). Therefore both imaging modalities are often considered as complementary in head and neck imaging [4], [30]. For diagnostic workup in tumor patients, CT protocols with higher tube currents (>50 mAs) should be used, and IV administration of an iodine-based contrast agent is always required [30]. To minimize the artifacts by metallic dental implants, primary axial thin-layer

**Figure 15: 74-year-old diabetic patient with acute onset of nerve palsy of the 3rd, 4th and 6th cranial nerves on the right side and progressive "reddening" of the right eye and painful eye movement.**
a) Axial CT demonstrates inflammatory changes of the right sphenoid sinus (arrow).
b) Sagittal reconstructed CT images demonstrate diffuse inflammatory changes of the globe and the optic nerve (arrow).
c) Coronal reconstructed CT images demonstrate subtle inflammatory changes also on the left side. MRI (not shown) demonstrated thrombosis of the cavernous sinus on both sides, which was not detectable on CT. Surgery confirmed Candida infection.



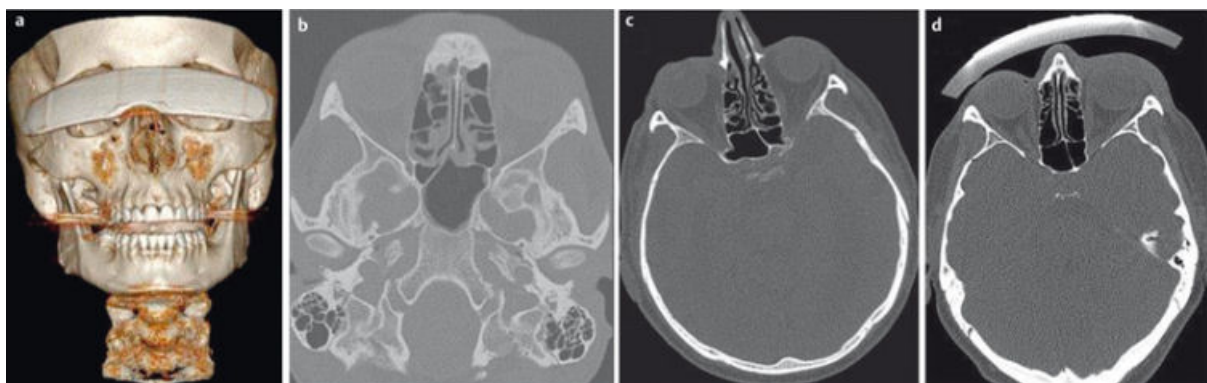**Figure 16: Impact of lens protection devices on image quality.**
a) 3D-VRT reconstruction. The lens protection device can be worn like glasses.
b) Standard CT protocol of the midface without lens protection.
c) Low-dose CT protocol without lens protection. Discrete increase of image noise.
d) Low-dose CT protocol with lens protection. There is no significant decrease of image quality. Lens exposure is reduced by 58%.

**Figure 17: Low-dose CT of the midface using a 64-row dual-source CT scanner.**
a) 18-year-old female patient who fell on her face. Coronal reconstructed image with 3 mm slice thickness. The fracture (arrow) can be assessed precisely.
b) 23-year-old patient with direct trauma to the head. Despite the lens protection device the fracture of the nasal bone is detected.
c) 47-year-old patient with facial swelling on the left side. The preseptal cellulitis (arrow) is detected despite the lens protection device.
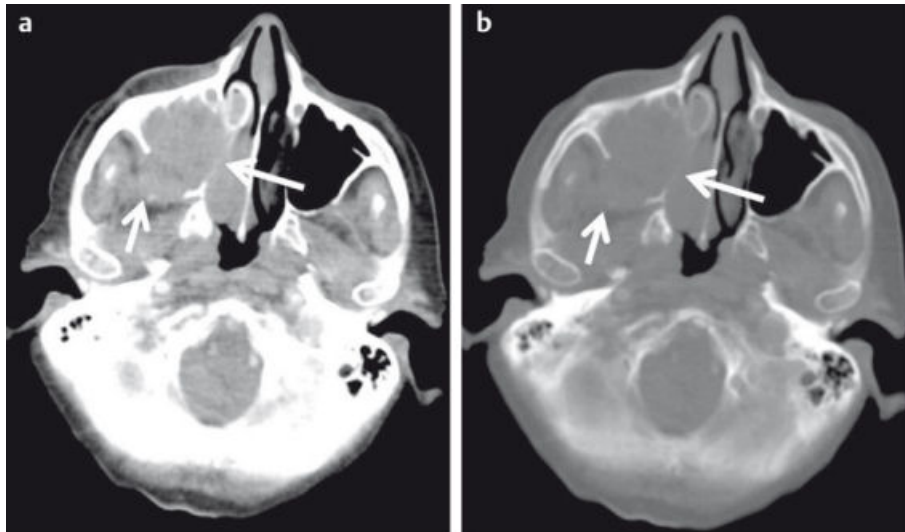


**Figure 18: Contrast-enhanced CT of the midface with squamous cell carcinoma of the right maxillary sinus.**
a) Axial image in bone window level setting. Complete opacification of the right maxillary sinus with tumor extension to the retromaxillary fossa (short arrow) and the nasal cavity. Infiltration of the medial wall of the maxillary sinus.
b) Infiltration of small bony structures can better be appreciated in bone window-level settings.

datasets with secondary multiplanar reconstruction (MPR) in bone and soft tissue window-level settings should be acquired [4].

The main task of imaging is to exactly describe the local tumor extent (Figure 19) and to detect possible lymph node and distant metastases [4], [30], [62].

Conventional CT imaging with static contrast agent administration mainly identifies morphological changes and provides anatomical information [63]. No conclusions regarding tumor physiology or biological behavior can be drawn. Perfusion CT (PCT) is a so-called functional imaging technique and allows noninvasive assessment of vascular architecture and the blood flow status of a tumor. It therefore offers quantifiable biomarkers [64].

Perfusion CT (PCT) relies on the sequential acquisition of CT images at a specific position or within a specific volume during the first passage of a bolus of contrast agent through the tissue. Contrast media induce a temporary increase in tissue density, and a time-density curve

(TDC) can be calculated for each voxel. Mathematical models are used to calculate several perfusion parameters, including blood flow (BF), blood volume (BV), mean transit time (MTT), and the so-called *permeability-surface area product* (PS) (Figure 20). The PS (in ml/min/100 g tissue) is a surrogate parameter for the presence of immature, neoangiogenetic vessels [64]. MTT (in sec) describes the average time the contrast agent needs for the first pass through the tissue. BV (in ml/100 g tissue) is a marker of the vascularity of the tumor, and BF (in ml/min/100 g tissue) allows quantification of blood flow within tumor [65].

In a retrospective study of 25 patients with advanced tumors, Hoefling et al. showed that there is a significant correlation between the PCT parameters and other relevant prognostic biomarkers [66]. Patients with lymph node metastases have a significantly poorer prognosis. However, identification of metastatic involvement of lymph nodes still relies on morphological criteria and is

**Figure 19: Contrast-enhanced CT of the midface of a 47-year-old patient after resection of a squamous cell carcinoma of the nasal cavity and new onset of epistaxis.**
a) Axial plane; recurrent disease with posterolateral infiltration of the sphenoid sinus and extension into the carotid canal (arrow).
b) Sagittal plane demonstrating osseous infiltration of the clivus (arrow).
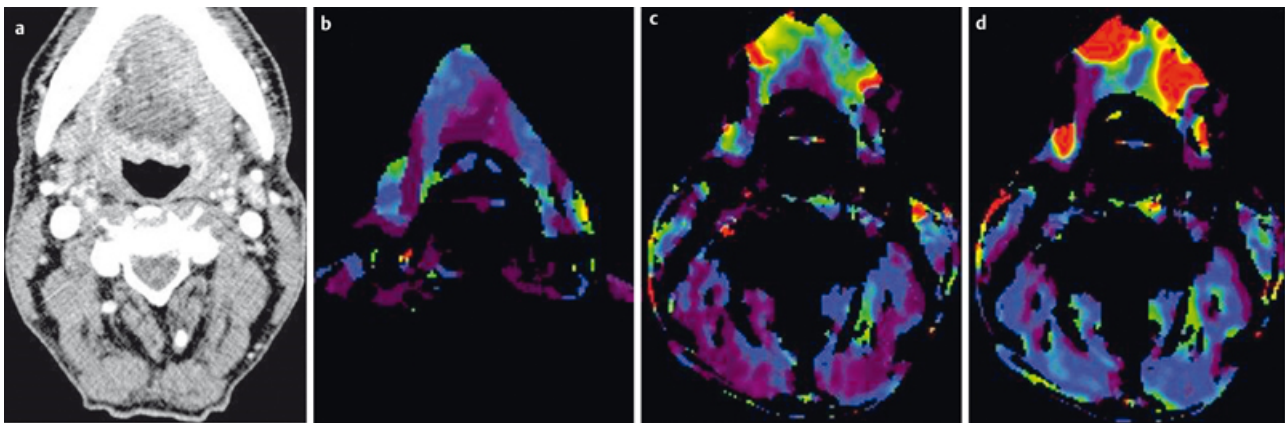c) Coronal plane with extension of the tumor into the pterygopalatine fossa (arrow).



**Figure 20: Perfusion-CT of a 51-year-old patient with lip carcinoma and newly diagnosed induration of the anterior floor of the mouth.**
a) Axial contrast-enhanced CT demonstrates discrete asymmetry and mild contrast enhancement on the left side.
b) PCT demonstrates increased blood volume,
c) increased blood flow
d) and increased permeability surface product indicating malignancy. Metastasis was confirmed by histology.

particularly difficult for lymph nodes <1 cm in diameter [67]. Bisdas et al. [68] and Trojanowska et al. [69] demonstrated that BF and BV are elevated in metastatic lymph nodes, though the difference to non-metastatic lymph nodes was statistically not significant in the study of Bisdas et al. Furthermore, PCT allows prognostically relevant characterization of the tumor with respect to its expected behavior during radiochemotherapy. Several studies suggest that there is a good correlation between increased BV and the response to radiochemotherapy [70], [71], [72], whereas low BF correlates with a poor response [73]. Another good correlation has been reported for the degree of malignancy and MTT [74]. Some authors recommend the use of PCT to monitor the effect of radio-chemotherapy [70], [71]. Since both postoperative changes and recurrent tumor display enhancement, differentiation between these two tissues can be difficult. In a retrospective study of Jin et al. [75], who investigated 48 patients with clinically suspected recurrence, an increase in BF identified recurrent tumor with 92.6% sensitivity and 96.3% specificity.

## 4.4 Orbit

Besides the detection of orbital complications of sinusitis (Figure 15, Figure 16), CT is mainly used for orbital imaging in the acute trauma setting. Due to the superior soft tissue contrast, MRI has replaced CT in tumor patients [76], [77]. This also applies to the diagnosis of retinoblastoma [78].

The diagnostic work-up of orbital trauma also requires high-resolution axial planes in bone and soft tissue window-level settings with multiplanar reconstruction (Figure 21) at least in axial and coronal planes [1], [11], [12]. It is very important to use thin-slice images with a decent overlap in order not to miss a fine fracture [33]. Particularly, the optic canal should be closely evaluated. In patients with complex fractures and roughly dislocated
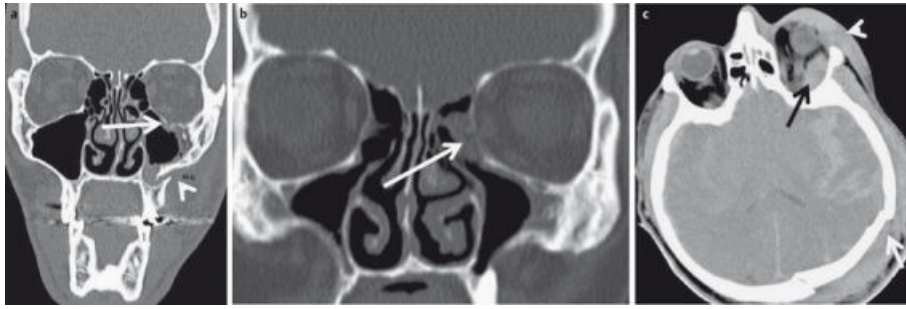
**Figure 21: CT of the midface for detection of orbital fractures.**
a) 23-year-old football player with direct trauma to the left face and new onset of diplopia. Fracture of the floor of the orbita (arrow) with herniation of extraconal fat.
b) 41-year-old patient with direct trauma to the globe. Fracture of the medial wall of the orbita and herniation of the medial rectus muscle (arrow).
c) 86-year-old patient with severe head injury and rapid onset of exophthalmos. Intraorbital extraconal hematoma (black arrow) and periorbital hematoma (arrowhead). Impression fracture of the skull (white arrow).
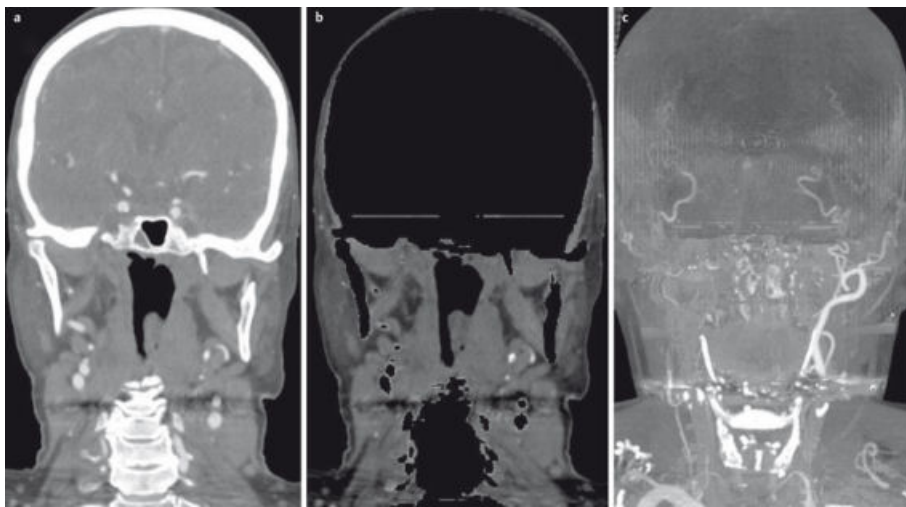


**Figure 22: Dual-source CT of the midface.**
a) Fusion image of the 80 kV and 120 kV datasets.
b) Automatic bone removal based on the different attenuation of bone in the two datasets.
c) MIP reconstruction of the automatically segmented vessels.

fragments, a 3D reconstruction can facilitate surgical treatment [12], [79]. IV administration of contrast agent is mandatory if inflammatory or infectious disease is suspected. Again, high-resolution thin slices in axial and coronal planes in soft tissue and bone window-level settings should be reconstructed with the latter being superior for the detection of osseous destruction.

A recent development in CT technology is the so-called dual-source CT (DSCT) scanner. With these CT scanners, the patient is examined by two different X-ray beams with different tube voltage. These beams can either be produced by separate X-ray tubes or by one tube with alternating tube voltages [80]. Because X-ray absorption within the tissue depends on tube voltage, two different datasets are generated, which can be further processed [81]. In addition to the automatic segmentation and removal of the bone (Figure 22) for CT angiography, the DSCT scanner can be used for a variety of other applications in head-neck imaging, offering for instance advanced tissue characterization [80] or dose reduction protocols. By combining the two sets of data, overall image quality and lesion detection can be improved as demonstrated by Tawfik et al. in a prospective study of 60 patients [82]. Wichmann et al. presented a prospective study of 170 patients who underwent a DSCT. The dataset acquired with 80 kV was comparable to the standard protocol with 120 kVA in terms of diagnostic accuracy while resulting in a significant reduction of radiation exposure [83].

# 5 FDG-PET/Computed tomography (FDG-PET/CT)

Positron emission tomography (PET) is an imaging procedure that allows imaging of metabolism in vivo using a radioactively labeled tracer. While CT and MRI detect pathologies on the basis of morphologic changes, PET can demonstrate pathological metabolism in organs that appear morphologically inconspicuous [84]. PET with fluorine-18-fluoro-deoxy-D-glucose (FDG) is an established technique for diagnosis, staging, and follow-up of patients
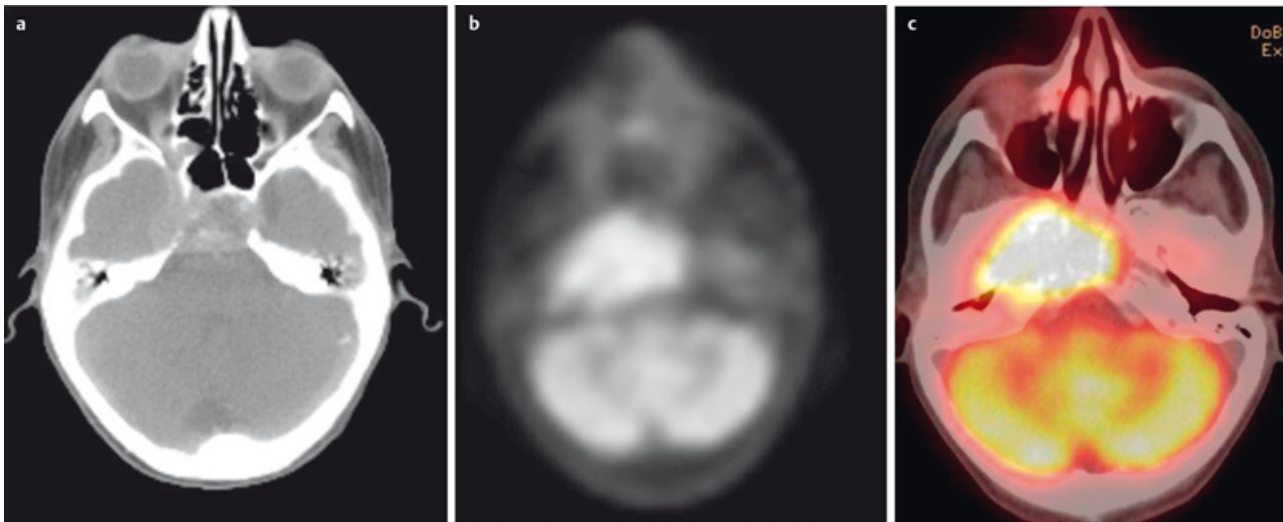
**Figure 23: FDG-PET/CT is a hybrid imaging technique which fuses functional PET data with high-resolution CT datasets.**
a) High-resolution CT for computation of attenuation-corrected images and precise anatomical localization of pathological metabolism.
b) Corresponding attenuation-corrected PET image.
c) Fusion-CT for anatomical correlation.

with tumors in the head and neck region [85], [86], [87], [88]. FDG is used as an analog for glucose in metabolism and is absorbed by the cells. Tumor cells usually have a higher metabolism than healthy cells, resulting in an increased uptake of FDG. Contrary to glucose, FDG is not further metabolized and therefore accumulates in tumor cells and can thus be detected. Usually, lesion characterization relies on the so-called SUV value (*standard uptake value*, SUV), which is a measure of the enrichment of the tracer within the lesion in relation to the total amount of tracer and the patient's body weight [84]. A SUV >2.5–3 is considered to indicate a malignant lesion [89]. Compared to CT imaging alone, higher sensitivities (86–100%) and specificities (69–87%) have been reported for FDG-PET [90], [91] in the detection of head and neck tumors or lymph node metastases. Due to the low spatial resolution, as well as the lack of anatomical landmarks, a precise anatomical mapping is often not possible, especially in the head and neck with its complex anatomy. FDG-PET/CT is a so-called hybrid imaging technique. The functional information of FDG-PET is combined with high spatial resolution CT using image fusion (Figure 23) to allow precise anatomical identification of the site of altered metabolism. Therefore, FDG-PET/CT has become an established imaging technique for the detection of primary tumors and lymph node or distant metastases and also for follow-up and monitoring of the treatment response [89], [92], [93].

Patients should fast before a FDG-PET/CT scan for 6 hours, and a blood glucose level <200 mg/dl immediately before the examination will ensure adequate uptake of FDG into tumor cells. The co-administration of IV insulin may help to reduce the risk of hyperglycemia but may also degrade image quality due to increased FDG storage in muscles and fat tissue. FDG-PET/CT examination of patients with hyperglycemia >200–250 mg/dl should

therefore be postponed, if possible, until there is a more favorable metabolic status [85], [93].

A typical whole-body FDG-PET/CT includes the area from the forehead to the mid-thigh. However, there is growing evidence that a dedicated examination protocol for the head and neck region (Figure 23) with a smaller field of view (FoV), thinner slices, and a longer recording time for the individual sections of the PET, so-called *high resolution head and neck PET/CT* (HR HN PET/CT), can improve diagnostic accuracy [93], [94]. The simultaneously acquired CT scan should be contrast enhanced [94].

FDG-PET/CT examinations are most beneficial for the detection of asymptomatic tumor recurrence (Figure 24) or posttherapeutic residual tumors [95], [96], [97]. In these cases, FDG-PET/CT has a very high sensitivity (90–100%) and a high negative predictive value [93], [98]. This is especially advantageous in patients with significantly altered anatomy after tumor resection and reconstructive surgery [89].

Scar formation, especially after extensive surgery, can be difficult to be differentiated from possible residual or recurrent tumor [99]. In a retrospective study of 123 patients by Dunsky et al. [95], FDG-PET/CT identified asymptomatic recurrence in 20% of all patients rated as disease-free by conventional CT. However, this increase in diagnostic yield did not lead to decreased mortality in their patient population. To avoid false positive results, it is crucial to have a distinct time interval between treatment and imaging. For radiochemotherapy, the majority of authors recommend a time interval of 12 weeks [89], [93], [100], [101], [102], and after surgery, the interval before imaging should be at least 4–6 weeks [98], [100]. Because surgical complications, e.g. abscess formation, can lead to false positive findings, interdisciplinary cooperation is necessary to avoid misdiagnosis [93]. FDG-PET/CT is also suitable for monitoring therapeutic response. Chen et al. demonstrated, in a prospective
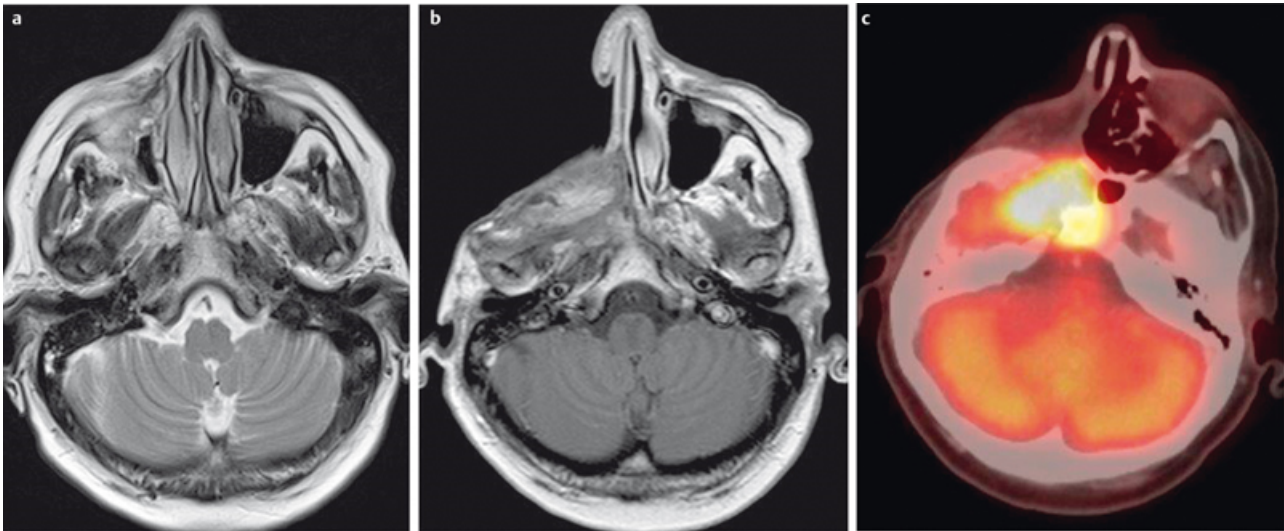
**Figure 24: 46-year-old female patient with chondrosarcoma of the right maxillary sinus.**
a) Preoperative axial T2w image demonstrates an inhomogeneous tumor with discrete infiltration of the surrounding soft tissue.
b) Contrast-enhanced T1w follow-up image demonstrating extensive scar formation which cannot be differentiated from recurrent tumor.
c) FDG-PET/CT performed the next day demonstrating increased metabolism within the scar formation, indicating recurrent disease, which was confirmed by surgery.
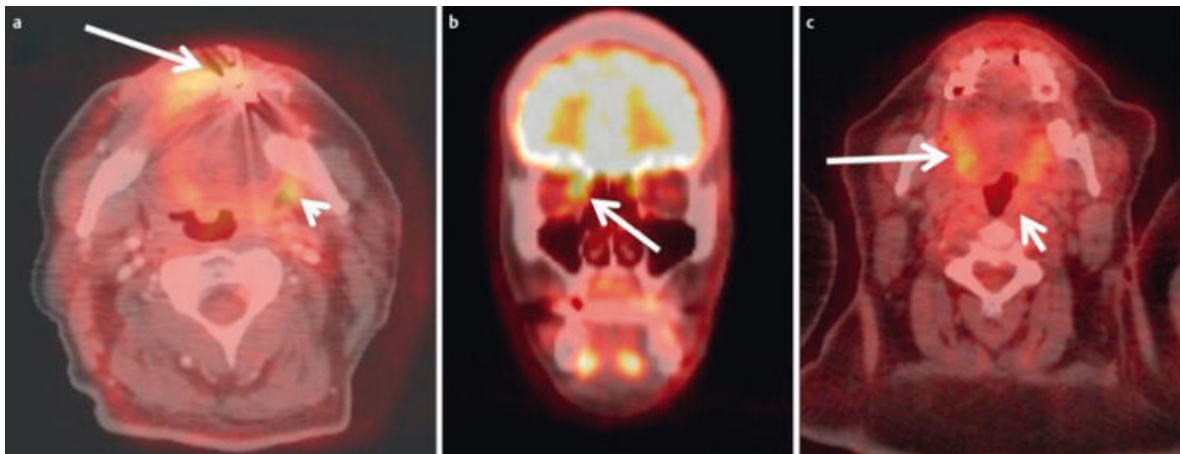


**Figure 25: Artifacts and pitfalls in FDG-PET/CT.**
a) 55-year-old patient with recurrent lip carcinoma. A malignant lesion in the left parapharyngeal space (short arrow) is suggested by misregistration caused by involuntary patient movement. The presumed tumor cannot be assessed in its entirety due to artifacts of metallic dental implants.
b) 41-year-old patient with intraorbital metastasis of a nasal squamous cell carcinoma. The tumor cannot be differentiated from the metabolically active medial rectus muscle.
c) 64-year-old female patient with CUP syndrome. Histologically proven carcinoma of the left pharyngeal tonsil. The SUV of the tumor was below the SUV of the intrinsic muscle of the tongue due to its low affinity to FDG.

study of 51 patients, that a reduction of SUV <0.64 compared to baseline value is associated with poor prognosis [103]. There is also a correlation between the prognosis and the preoperative SUV of the tumor or the ipsilateral [104] and contralateral [105] lymph nodes. A tumor SUV >8.5 preoperatively is associated with a significantly increased risk of recurrence [105].

Because FDG is not a tumor-specific tracer, there is a potential risk of misdiagnosis related to artifacts (Figure 25). False positive results may occur due to misregistration of FDG-PET and CT caused by patient movements [85], [89], [93] as well as a low affinity of the tumor to the tracer [93] or a tumor size below the spatial resolu-

tion of the PET detector [85]. Especially in the midface and the paranasal sinuses, masking of a tumor by artifacts of metal-containing dental implants or close spatial relation to highly FDG-affine tissue, such as the brain or the extra-ocular eye muscles (Figure 25), may occur [93]. Perineural tumor spread can also be identified by FDG-PET/CT. However, its role for this disease entity in comparison to MR imaging has yet to be defined [106].

# 6 Magnetic resonance imaging (MRI)

MRI relies on the excitation of hydrogen protons in tissues by a high-frequency radiopulse while the patient lies inside a magnetic field. The resulting signals are then registered using a special antenna, the so-called coil. In contrast to CT, tissues are not characterized and differentiated by densities measured in Hounsfield units, but on the basis of their signal intensities in the differently weighted images. A basic distinction is made between T1-weighted (T1w) and T2-weighted (T2w) images (Figure 26). Tissue contrasts can be enhanced by intravenous contrast agents. The standard MR contrast agents are gadolinium-based and induce a T1 signal increase of tissues that accumulate them. With dedicated excitation pulses, the signal from fat, which is hyperintense (= bright) on both T1w and T2w images, can be suppressed (so-called fat saturation). This technique can be used to enhance the conspicuity of edema on T2w images or to emphasize contrast enhancement on T1w images. Diffusion-weighted imaging (DWI) techniques allow the detection and quantification of water diffusion in vivo (Figure 27) and contribute additional information for tissue characterization [107].

The midface should always be imaged with a dedicated head-neck coil [8] while the orbit can be imaged using either a small loop surface coils or the head coil alone or in combination with a surface coil [108]. Surface coils allow a smaller field of view with increased spatial resolution, while the head coil provides a more homogenous signal and allows the simultaneous assessment of the contralateral orbit.

## 6.1 Fractures

Because of their low content of water, cortical bone appear as hypointense (= dark) structures. With exception of the skull base, bony structures of the midface and orbit are too thin to be evaluated by MRI. Therefore MR imaging is the imaging modality of choice in the acute trauma setting [109]. However, T2w images with fat suppression are superior compared to CT for the detection of posttraumatic lesions of the optic nerve [79].

## 6.2 Tumors of the midface

MRI is superior to CT for the differentiation between inflammatory changes and tumor [61]. Inflammatory changes, as well as retained secretions, appear very bright on T2w images due to their high water content [110]. In contrast, due to their high cellularity, most midface tumors appear hypointense on T2w sequences and have an intermediate signal on T1w images [3], [4], [61], [110]. These tumors show significant enhancement after contrast administration (Figure 26). However, there is often a significant overlap between the imaging appearance of benign and malignant tumors [111]. An ADC parameter map (*apparent diffusion coefficient*, ADC) computed from DWI [112] may improve the diagnostic accuracy of MRI. A low ADC (Figure 28) indicates restricted diffusion of water in the tissue, which correlates with tumor cellularity [113]. Therefore, malignant tumors have a significantly lower ADC value ($0.87 \pm 0.32 \times 10^3$ mm$^2$/s) compared to benign tumors ($1.35 \pm 0.29 \times 10^3$ mm$^2$/s) or inflammatory changes ($1.50 \pm 0.5 \times 10^{-3}$ mm$^2$/s), as demonstrated by Sasaki et al. in a retrospective study of 61 patients [114]. DWI also allows the detection of lymph node metastases before morphological changes become apparent on anatomical MR images. In a prospective study of 301 histologically analyzed lymph nodes, Vandecaveye et al. [115] found 94% sensitivity and 97% specificity for the detection of metastatic lymph nodes <1 cm in diameter using an ADC cut-off value $<0.94 \times 10^{-3}$ mm$^2$/s. These findings were confirmed in a prospective study of Barchetti et al. [116] including 239 histologically analyzed lymph nodes. They reported comparable sensitivity and specificity for MR imaging at 3T.

In general, MRI does not allow histological classification of lesions [4]. However, a hyperintense tumor on non-enhanced T1w images (Figure 29) makes malignant melanoma the most likely diagnosis. The signal increase in unenhanced T1w images is related to the paramagnetic effects of melanin and is therefore more common in melanotic than in amelanotic tumors [117].

Osseous infiltration of the skull base is better detected by MR imaging than by CT [118]. Particularly, the hyperintense signal of fatty bone marrow should be carefully evaluated to identify areas of low signal intensity as a sign of bone marrow infiltration by tumor on T1w and Tw2 images (Figure 30) [61]. Other common imaging features of osseous infiltration are hyperintense bone marrow signal on T2w images with fat saturation and contrast enhancement [61], which is best appreciated on T1w images with fat saturation.

Intraorbital and intracranial tumor extension can also be better assessed by MR imaging [4]. Linear enhancement of the dura may indicate a reaction to adjacent tumor growth. Nodular enhancement or thickening of the dura >5 mm, on the other hand, indicates dural infiltration with 100% sensitivity and 91% specificity [119] while pial enhancement is the positive proof. Abnormal signal intensities in the extraocular muscles (100%) on T2w images have the highest positive predictive value for orbital infiltration, followed by stranding of orbital fatty tissue (80%) [120], [121], [122].

A new onset of cranial nerve palsy in patients with known malignancy of the midface is highly suspicious of perineural tumor *spread* (PNS). Neurological symptoms rarely occur before detection of the primary tumor. MRI is the imaging modality of choice for detecting of PNS. Typical imaging findings (Figure 31) are loss of fat signal in the foramina of the skull base or the pterygopalatine fossa, enhancement of the affected nerve after contrast administration, and, in advanced stages, widening of the foramina or atrophy of the muscles of mastication due to denervation [123].
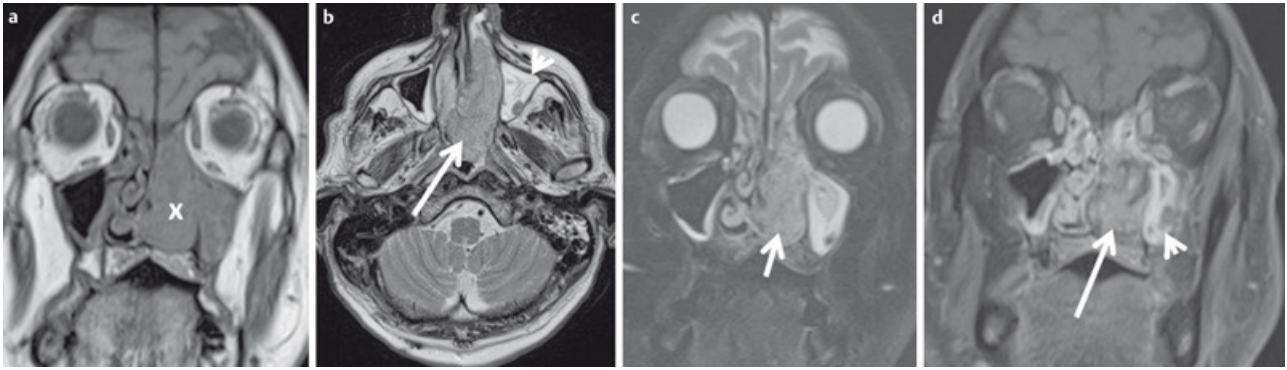
**Figure 26: MRI of a 65-year-old patient with histologically proven squamous cell carcinoma of the nasal cavity.**
a) Coronal T1w image. The tumor (x) is iso-intense to muscle, fat tissue is hyperintense on T1w images.
b) Axial T2w image. The tumor is hyperintense to muscle. MRI allows differentiation between hyperintense retention within the maxillary sinus and the tumor.
c) Coronal T2w image with fat suppression. With fat tissue appearing hypointense, tumor and inflammatory changes of the maxillary sinus are better delineated.
d) Coronal contrast-enhanced T1w images with fat suppression. Contrast enhancement is better delineated with fat suppression. The tumor (arrow) enhances avidly but less compared to normal mucosa (arrowhead).
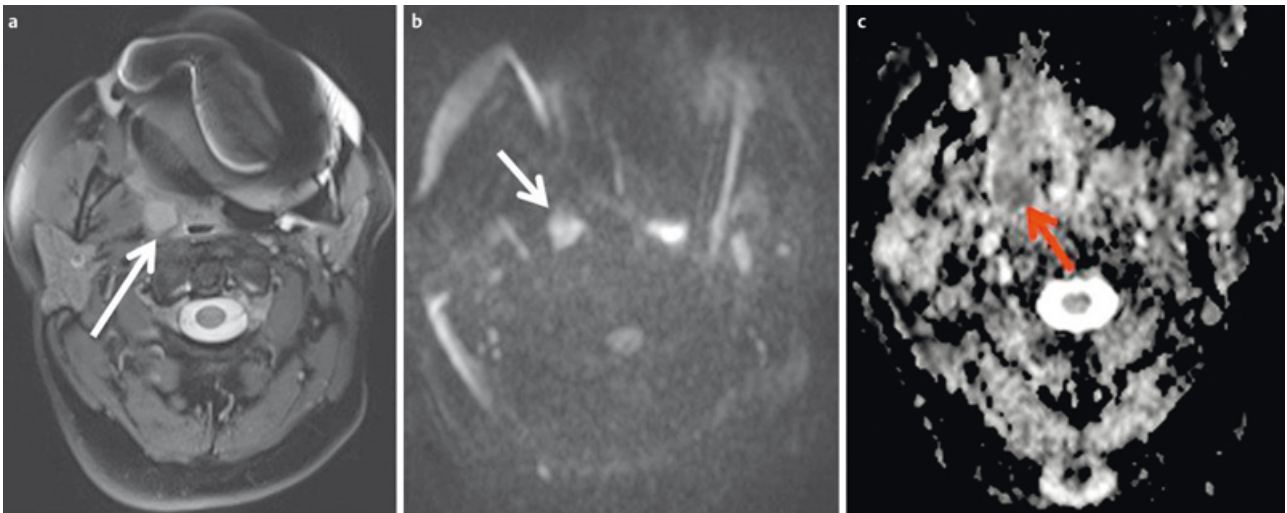


**Figure 27: 49-year-old patient after resection of a lip carcinoma on the right side.**
a) Axial T2w images demonstrate a solitary retropharyngeal lymph node (arrow). Significant artifacts due to metallic dental implants.
b) The lymph node (arrow) appears hyperintense on diffusion-weighted images.
c) The lymph node (arrow) appears hypointense on the ADC map. Calculated ADC was $0.65 \times 10^{-3}$ mm$^2$/s, indicating malignancy. This was confirmed by histology.



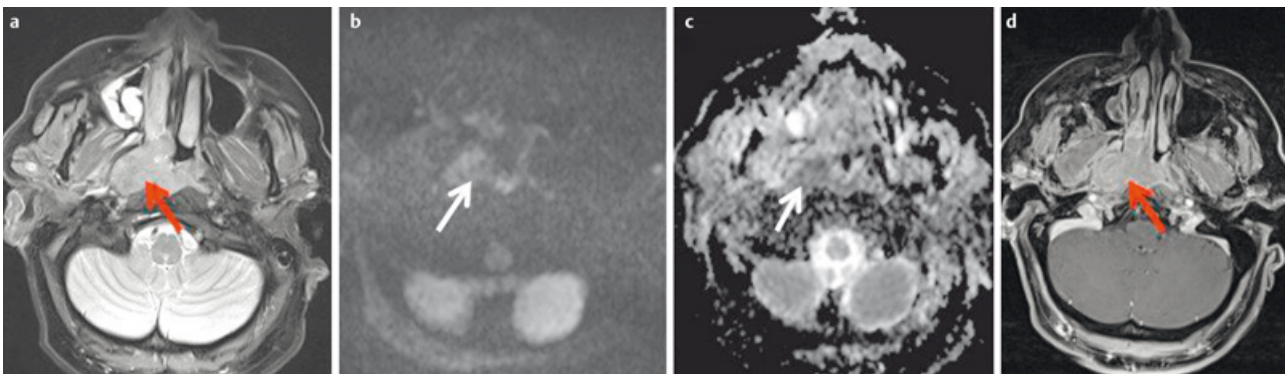**Figure 28: MRI of a 66-year-old patient with a nasal cavity carcinoma extending into the nasopharynx.**
a) There is marked enhancement on contrast-enhanced T1w image with fat saturation.
b) Axial T2w images demonstrate a homogeneous, discretely hypointense tumor (arrow).
c) The tumor is hypointense on the ADC-map and the calculated ADC-value is $0.51 \times 10^{-3}$ mm$^2$/s. Histologically confirmed squamous cell carcinoma.
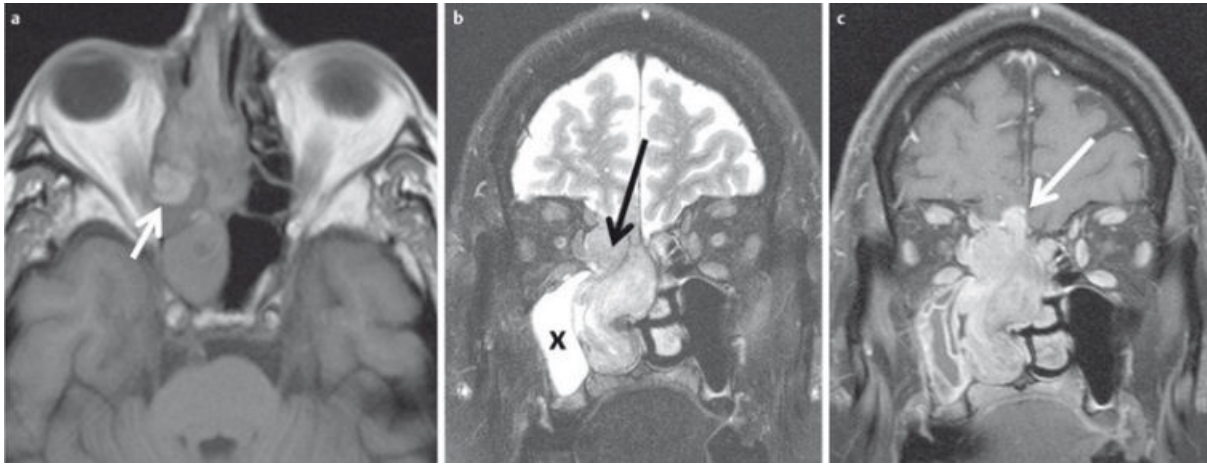
**Figure 29: 48-year-old patient with histologically confirmed malignant melanoma of the right nasal cavity.**
a) The tumor appears hyperintense on plain T1w images.
b) On T2w images the tumor is inhomogeneously hyperintense and can be clearly differentiated from the hyperintense inflammatory changes of the right maxillary sinus (x).
c) The tumor enhances avidly after contrast administration, and there is intracranial tumor growth through the cribriform plate.
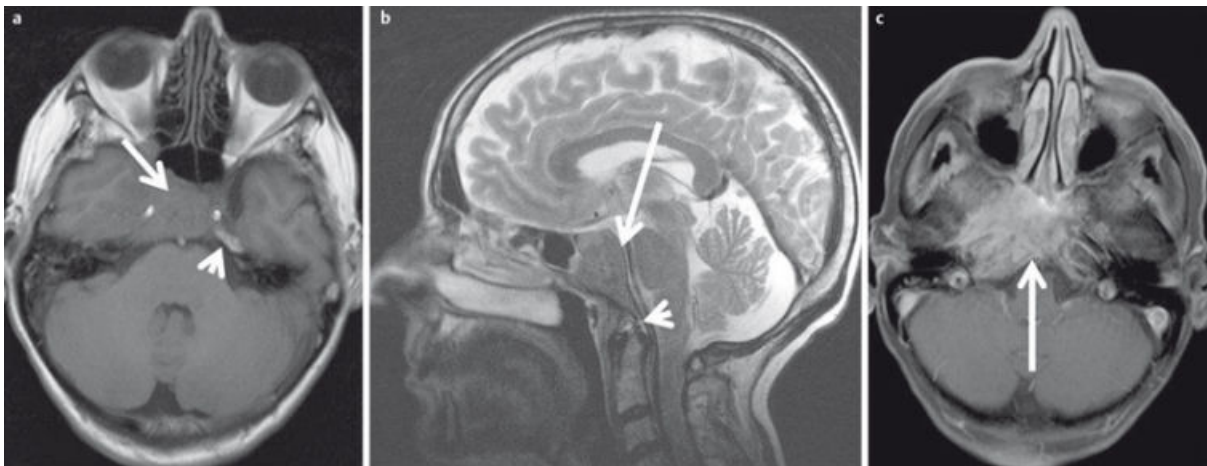


**Figure 30: 53-year-old patient with squamous cell carcinoma of the nasal cavity and osseous infiltration of the skull base.**
a) On T1w images the hypointense tumor (arrow) replaces the hyperintense fatty marrow of the skull base (arrowhead).
b) On sagittal T2w images (arrow) the tumor also appears hypointense compared to bone marrow (arrowhead).
c) There is avid enhancement after contrast administration.
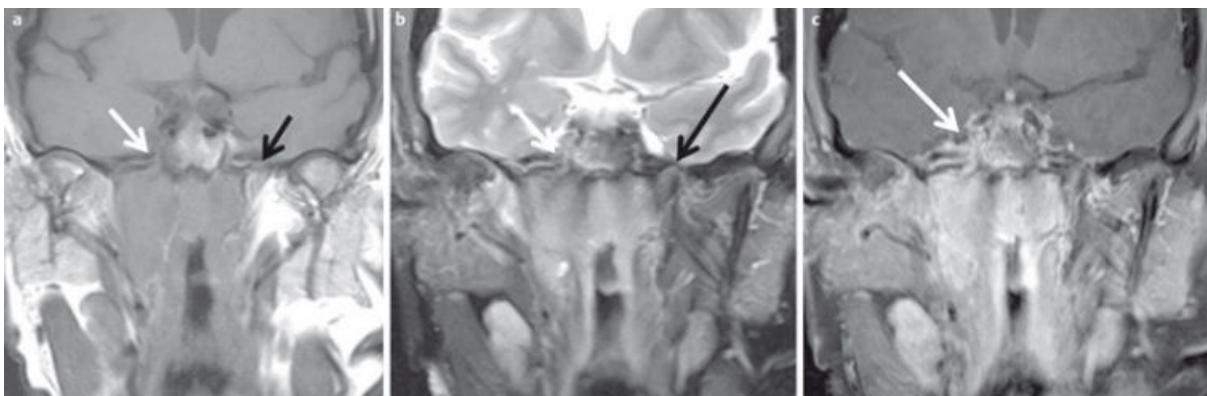


**Figure 31: MRI criteria of perineural tumor spread. 62-year-old patient with histologically proven carcinoma of the anterior ethmoid cells and new onset of facial pain on the right side.**
a) Coronal T1w images with loss of fat signal (white arrow) of the oval foramen in comparison to contralateral side (black arrow).
b) Hyperintense signal on T2w images with fat suppression of the oval foramen (arrow) in comparison to contralateral side (dotted arrow).
c) Avid enhancement within the oval foramen on the right side (arrow), which is widened compared to the contralateral side.
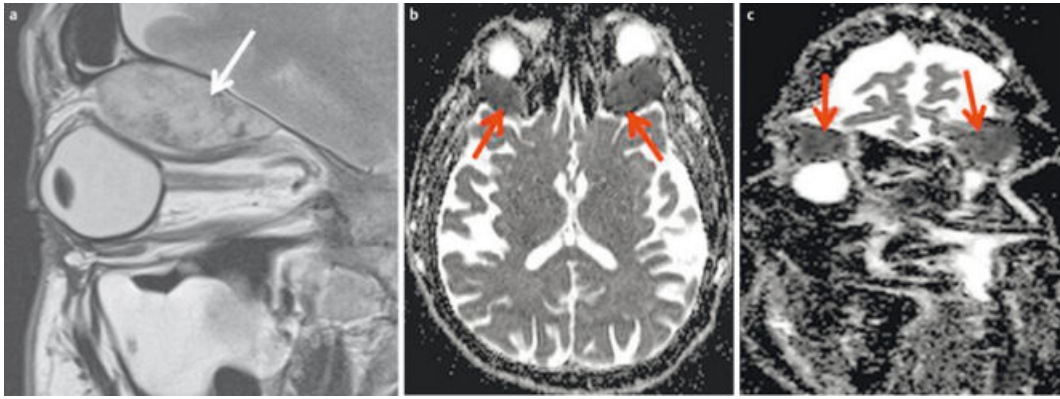
**Figure 32: 44-year-old patient with new onset of diplopia and progressive loss of vision in both eyes.**
a) T2w images demonstrate a subperiostal inhomogeneous lesion with smooth margins.
b) Axial ADC map demonstrates bilateral lesions (arrow). ADC-value is >1.0×10$^{-3}$ mm$^2$/s on both sides, indicating a benign lesion (histologically proven hematoma due to coagulopathy).
c) Coronal ADC map with significant distortion artifacts due to air-tissue interfaces and involuntary eye movement.



**Figure 33: 4-month-old child with new orbital swelling and fever after sinusitis.**
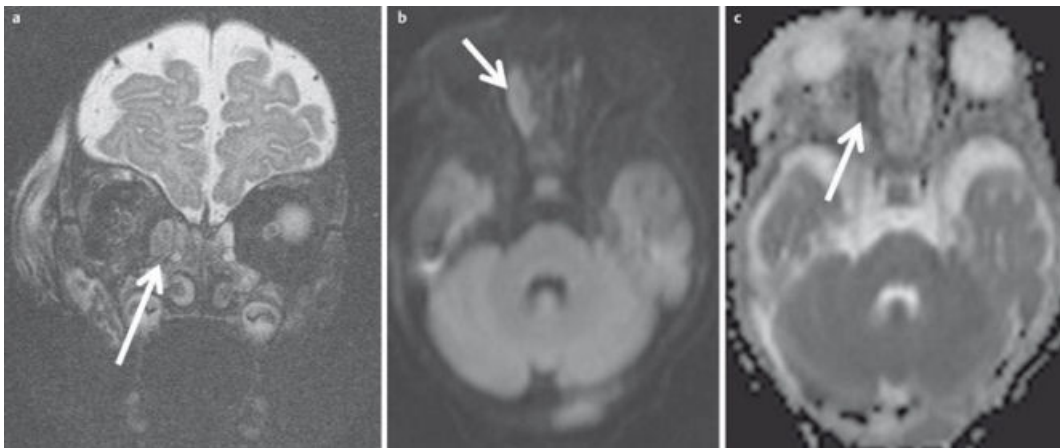a) Coronal T2w images with fat saturation demonstrate a small hyperintense lesion at the medial aspect of the orbital wall. There are no signs of orbital cellulitis.
b) The lesion appears hyperintense on diffusion-weighted images.
c) and hypointense on the ADC-map, indicating abscess formation. This was confirmed by surgery.

Early scar formation and recurrence or residual tumor may exhibit similar contrast enhancement and can therefore pose a diagnostic dilemma for conventional MRI. DWI may overcome this limitation. In a prospective study of 32 patients with known recurrent tumor, Abdel Razek et al. [107] showed that an ADC <1.3×10$^{-3}$ mm$^2$/s indicates recurrent disease with 84% sensitivity and 90% specificity and a positive predictive value of 94%.

DWI may also predict the clinical course. Lambrecht et al. [124] postulate that pretherapeutic ADC is an independent prognostic factor for survival of patients with midface tumors. They prospectively examined 161 patients with a median follow-up period of 50 months. Similar results were found by Nakajo et al. [125] in their prospective study of 26 patients. An ADC value <0.88×10$^{-3}$ mm$^2$/s significantly correlates with an unfavorable clinical outcome. The predictive value is comparable to that of a markedly increased SUV in FDG-PET/CT at baseline.

## 6.3 Orbit

With its excellent soft tissue contrast, MRI is the modality of choice for imaging the orbit [77]. Benign and malignant orbital lesions also have a significant overlap of morphological criteria. DWI may improve the differentiation of benign and malignant orbital lesions. Based on a prospective study of 47 patients, Sepahdari et al. [126] defined an ADC value <1.0×10$^{-3}$ mm$^2$/s as a cut-off for the differentiation between benign and malignant lesions with 64% sensitivity and 84% specificity. In particular, lesions which appear hypointense in T2-weighted images (Figure 32) can be better differentiated. Fatima et al. identified a different cut-off of 0.84×10$^{-3}$ mm$^2$/s in their prospective study of 39 patients. With this corrected threshold, they differentiated benign and malignant lesions with 83% sensitivity and 86% specificity [127]. DWI is also suitable to distinguish orbital cellulitis from abscess formation (Figure 33) at an early stage [128]. In patients with an endocrine orbitopathy, the ADC value can be used as a
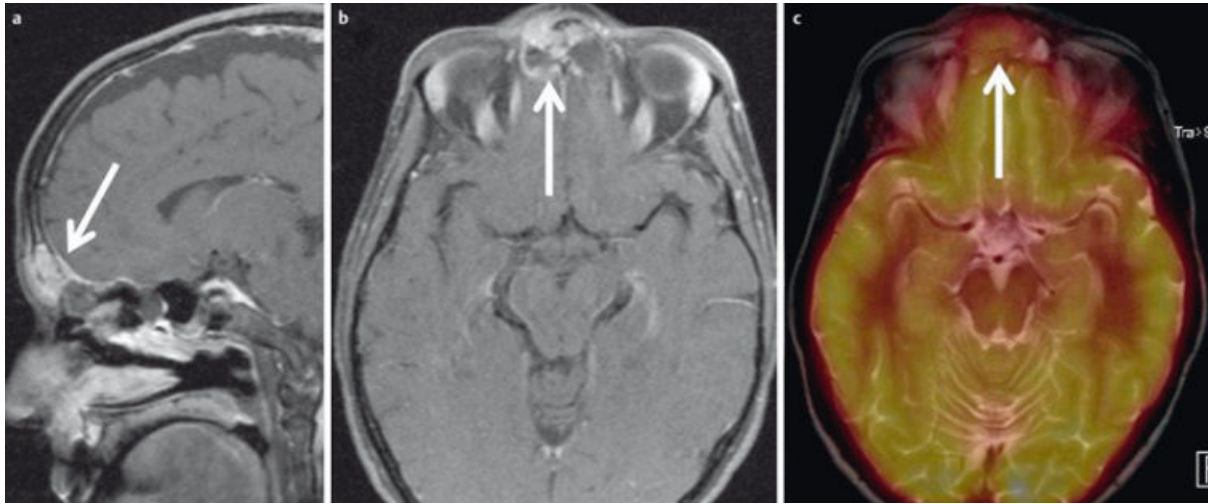
**Figure 34: FDG-PET/MRI of a 47-year-old female patient with a 3-month history of pressure sensation in the frontal head.**
a) Sagittal contrast-enhanced T1w images showing an enhancing tumor within the frontal sinus and linear enhancement of the mildly thickened dura (arrow).
b) The posterior and anterior cortical bone of the frontal sinus is thinned by the tumor and there is intracranial tumor growth (arrow).
c) FDG-PET/MRI demonstrates significantly increased metabolism. Histologically proven Ewing sarcoma.

quantifiable biomarker for assessing disease activity, as Politi et al. demonstrated in a prospective study [129].

A major limitation of orbital DWI is the vulnerability to artifacts [130], either caused by eye movement or at the interface to the aerated paranasal sinuses (Figure 32). This limitation can be overcome by using optimized sequences, allowing reliable ADC quantification of lesions in the orbital space [131].

MRI also allows perfusion weighted imaging. This can be performed as T2w Dynamic susceptibility contrast enhanced (DSCE) imaging, which is comparable to PCT, and as T1w contrast enhanced imaging [132]. A recent meta-analysis by Bernstein et al. demonstrated a good correlation between MR-derived perfusion parameters and clinical outcome [133]. However, PWI of the midface and orbit is also limited by severe artifacts. Therefore, it is not an established imaging technique in clinical routine [133].

# 7 FDG-PET/Magnetic resonance imaging (FDG-PET/MRI)

The wider availability of FDG-PET/MR systems (Figure 34) has increased the use of this modality for the diagnostic assessment of head and neck tumors [134]. Theoretical advantages over FDG-PET/CT are the better soft-tissue contrast of MRI [135] and the option of combining PET information with functional MRI techniques, such as DWI [136]. Especially in the midface, FDG-PET/MRI has the added advantage of being less susceptible to artifacts caused by metallic dental implants [137]. Partovi et al. studied 14 patients who had undergone FDG-PET/CT and FDG-PET/MRI and found no significant difference in terms of diagnostic accuracy [138]. In another study, fusion of DWI data with FDG-PET data was found to have no impact on diagnostic yield [139]. In a study of lymph node metastases in 12 patients, FDG-PET/MRI had 80% sensitivity versus 70% for MRI alone [140].

Although the availability of these hybrid systems is increasing, their number is still small. Therefore, the role of FDG-PET/MRI in the diagnostic evaluation of head and neck tumors remains to be defined in further studies [135].

# Summary

Conventional radiography has been replaced by computed tomography (CT) and magnetic resonance imaging (MRI) in the diagnostic evaluation of the midface and orbit.

Low-dose CT is the imaging modality of choice in patients with chronic rhinosinusitis. Alternatively, digital volume tomography can be used. However, scientific evidence is still sparse, and no specific recommendations for its use have been made by the major societies.

For all other conditions, axial CT datasets should be acquired with secondary reconstruction in axial and coronal planes in the soft tissue and bone window-level setting. Use of an IV contrast agent is required for assessing inflammatory and neoplastic conditions. The role of perfusion CT in the routine clinical setting remains to be defined.

Eye protection should be used to decrease radiation exposure to the lens.

FDG-PET/CT is the imaging modality of choice for patients with recurrent disease or for patients with cancer of unknown primary.

MRI is the modality of choice for imaging the orbit, except in the acute trauma setting and for the detection of intracranial complications of inflammatory or neoplastic conditions of the midface.

Due to limited availability, the role of FDG-PET/MRI in head and neck imaging has to be further evaluated.

With the use of all imaging modalities, interdisciplinary cooperation is the key to avoiding unnecessary examinations and misdiagnosis.

# Competing interests

The author declares that he has no competing interests.

# References

1. Caranci F, Cicala D, Cappabianca S, Briganti F, Brunese L, Fonio P. Orbital fractures: role of imaging. Semin Ultrasound CT MR. 2012 Oct;33(5):385-91. DOI: 10.1053/j.sult.2012.06.007

2. Hopper RA, Salemy S, Sze RW. Diagnosis of midface fractures with CT: what the surgeon needs to know. Radiographics. 2006 May-Jun;26(3):783-93. DOI: 10.1148/rg.263045710

3. Eggesbø HB. Radiological imaging of inflammatory lesions in the nasal cavity and paranasal sinuses. Eur Radiol. 2006 Apr;16(4):872-88. DOI: 10.1007/s00330-005-0068-2

4. Eggesbø HB. Imaging of sinonasal tumours. Cancer Imaging. 2012;12:136-52. DOI: 10.1102/1470-7330.2012.0015

5. Bacher K, Smeets P, Bonnarens K, De Hauwere A, Verstraete K, Thierens H. Dose reduction in patients undergoing chest imaging: digital amorphous silicon flat-panel detector radiography versus conventional film-screen radiography and phosphor-based computed radiography. AJR Am J Roentgenol. 2003 Oct;181(4):923-9. DOI: 10.2214/ajr.181.4.1810923

6. Strotzer M, Gmeinwieser JK, Völk M, Fründ R, Seitz J, Feuerbach S. Detection of simulated chest lesions with normal and reduced radiation dose: comparison of conventional screen-film radiography and a flat-panel x-ray detector based on amorphous silicon. Invest Radiol. 1998 Feb;33(2):98-103.

7. AWMF. Radiologische Diagnostik im Kopf-Hals-Bereich. Leitlinien der Deutschen Röntgengesellschaft (DRG). 2014 [cited 05.08.2014]. (AWMF Leitlinien-Register; 039-093).

8. Dammann F, Bootz F, Cohnen M, Hassfeld S, Tatagiba M, Kösling S. Diagnostic imaging modalities in head and neck disease. Dtsch Arztebl Int. 2014 Jun;111(23-24):417-23. DOI: 10.3238/arztebl.2014.0417

9. Konen E, Faibel M, Kleinbaum Y, Wolf M, Lusky A, Hoffman C, Eyal A, Tadmor R. The value of the occipitomental (Waters') view in diagnosis of sinusitis: a comparative study with computed tomography. Clin Radiol. 2000 Nov;55(11):856-60. DOI: 10.1053/crad.2000.0550

10. Kim SH, Ahn KJ, Lee JM, Choi KH, Han SH. The usefulness of orbital lines in detecting blow-out fracture on plain radiography. Br J Radiol. 2000 Dec;73(876):1265-9. DOI: 10.1259/bjr.73.876.11205669

11. Lee HJ, Jilani M, Frohman L, Baker S. CT of orbital trauma. Emerg Radiol. 2004 Feb;10(4):168-72. DOI: 10.1007/s10140-003-0282-7

12. Uzelac A, Gean AD. Orbital and facial fractures. Neuroimaging Clin N Am. 2014 Aug;24(3):407-24, vii. DOI: 10.1016/j.nic.2014.03.008

13. Miracle AC, Mukherji SK. Conebeam CT of the head and neck, part 1: physical principles. AJNR Am J Neuroradiol. 2009 Jun;30(6):1088-95. DOI: 10.3174/ajnr.A1653

14. Cakli H, Cingi C, Ay Y, Oghan F, Ozer T, Kaya E. Use of cone beam computed tomography in otolaryngologic treatments. Eur Arch Otorhinolaryngol. 2012 Mar;269(3):711-20. DOI: 10.1007/s00405-011-1781-x

15. Leiva-Salinas C, Flors L, Gras P, Más-Estellés F, Lemercier P, Patrie JT, Wintermark M, Martí-Bonmatí L. Dental flat panel conebeam CT in the evaluation of patients with inflammatory sinonasal disease: Diagnostic efficacy and radiation dose savings. AJNR Am J Neuroradiol. 2014 Nov-Dec;35(11):2052-7. DOI: 10.3174/ajnr.A4019

16. Rottke D, Patzelt S, Poxleitner P, Schulze D. Effective dose span of ten different cone beam CT devices. Dentomaxillofac Radiol. 2013;42(7):20120417. DOI: 10.1259/dmfr.20120417

17. Angelopoulos C. Cone beam tomographic imaging anatomy of the maxillofacial region. Dent Clin North Am. 2008 Oct;52(4):731-52, vi. DOI: 10.1016/j.cden.2008.07.002

18. Miracle AC, Mukherji SK. Conebeam CT of the head and neck, part 2: clinical applications. AJNR Am J Neuroradiol. 2009 Aug;30(7):1285-92. DOI: 10.3174/ajnr.A1654

19. Bremke M, Wiegand S, Sesterhenn AM, Eken M, Bien S, Werner JA. Digital volume tomography in the diagnosis of nasal bone fractures. Rhinology. 2009 Jun;47(2):126-31.

20. Choudhary AB, Motwani MB, Degwekar SS, Bhowate RR, Banode PJ, Yadav AO, Panchbhai A. Utility of digital volume tomography in maxillofacial trauma. J Oral Maxillofac Surg. 2011 Jun;69(6):e135-40. DOI: 10.1016/j.joms.2010.07.081

21. Yilmaz SY, Misirlioglu M, Adisen MZ. A Diagnosis of Maxillary Sinus Fracture with Cone-Beam CT: Case Report and Literature Review. Craniomaxillofac Trauma Reconstr. 2014 Jun;7(2):85-91. DOI: 10.1055/s-0034-1371550

22. Fakhran S, Alhilali L, Sreedher G, Dohatcu AC, Lee S, Ferguson B, Branstetter BF 4th. Comparison of simulated cone beam computed tomography to conventional helical computed tomography for imaging of rhinosinusitis. Laryngoscope. 2014 Sep;124(9):2002-6. DOI: 10.1002/lary.24603

23. Brenner DJ, Hall EJ. Computed tomography – an increasing source of radiation exposure. N Engl J Med. 2007 Nov;357(22):2277-84. DOI: 10.1056/NEJMra072149

24. Sohaib SA, Peppercorn PD, Horrocks JA, Keene MH, Kenyon GS, Reznek RH. The effect of decreasing mAs on image quality and patient dose in sinus CT. Br J Radiol. 2001 Feb;74(878):157-61. DOI: 10.1259/bjr.74.878.740157

25. Brem MH, Zamani AA, Riva R, Zou KH, Rumboldt Z, Hennig FF, Kikinis R, Norbash AM, Schoepf UJ. Multidetector CT of the paranasal sinus: potential for radiation dose reduction. Radiology. 2007 Jun;243(3):847-52. DOI: 10.1148/radiol.2433050207

26. Paul J, Jacobi V, Farhang M, Bazrafshan B, Vogl TJ, Mbalisike EC. Radiation dose and image quality of X-ray volume imaging systems: cone-beam computed tomography, digital subtraction angiography and digital fluoroscopy. Eur Radiol. 2013 Jun;23(6):1582-93. DOI: 10.1007/s00330-012-2737-2

27. Rudman KL, O'Brien EK, Leopold DA. Radiographic distribution of drops and sprays within the sinonasal cavities. Am J Rhinol Allergy. 2011 Mar-Apr;25(2):94-7. DOI: 10.2500/ajra.2011.25.3569

28. Alsufyani NA, Noga ML, Finlay WH, Major PW. Topical contrast agents to improve soft-tissue contrast in the upper airway using cone beam CT: a pilot study. Dentomaxillofac Radiol. 2013;42(7):20130022. DOI: 10.1259/dmfr.20130022

29. AWMF. Dentale digitale Volumentomographie. Leitlinien der Deutschen Gesellschaft für Zahn-, Mund- und Kieferheilkunde (DGZMK). 2014 [cited 03.08.2014]. (AWMF Leitlinien-Register; 083-005).

30. Walden MJ, Aygun N. Head and neck cancer. Semin Roentgenol. 2013 Jan;48(1):75-86. DOI: 10.1053/j.ro.2012.09.002

31. Stiller W. Grundlagen der Mehrzeilendetektor-Computertomographie : Teil 1: Technischer Aufbau und physikalisch-technische Grundlagen [Principles of multidetector-row computed tomography : part 1. Technical design and physicotechnical principles]. Radiologe. 2011 Jul;51(7):625-37. DOI: 10.1007/s00117-011-2189-8

32. Stiller W. Grundlagen der Mehrzeilendetektor-Computertomographie. Teil 2: Einflussfaktoren der Strahlenexposition und aktuelle technische Entwicklungen [Principles of multidetector-row computed tomography. Part 2: determinants of radiation exposure and current technical developments]. Radiologe. 2011 Dec;51(12):1061-76. DOI: 10.1007/s00117-011-2244-5

33. Fishman EK, Ney DR, Heath DG, Corl FM, Horton KM, Johnson PT. Volume rendering versus maximum intensity projection in CT angiography: what works best, when, and why. Radiographics. 2006 May-Jun;26(3):905-22. DOI: 10.1148/rg.263055186

34. Bernhardt TM, Rapp-Bernhardt U, Fessel A, Ludwig K, Reichel G, Grote R. CT scanning of the paranasal sinuses: axial helical CT with reconstruction in the coronal direction versus coronal helical CT. Br J Radiol. 1998 Aug;71(848):846-51. DOI: 10.1259/bjr.71.848.9828797

35. MacLennan AC. Radiation dose to the lens from coronal CT scanning of the sinuses. Clin Radiol. 1995 Apr;50(4):265-7.

36. Langner S, Stumpe S, Kirsch M, Petrik M, Hosten N. No increased risk for contrast-induced nephropathy after multiple CT perfusion studies of the brain with a nonionic, dimeric, iso-osmolal contrast medium. AJNR Am J Neuroradiol. 2008 Sep;29(8):1525-9. DOI: 10.3174/ajnr.A1164

37. Sohns JM, Staab W, Sohns C, Schwarz A, Streit U, Hosseini AS, Spiro JE, Kertész A, Zwaka PA, Lotz J. Current perspective of multidetector computed tomography (MDCT) in patients after midface and craniofacial trauma. Clin Imaging. 2013 Jul-Aug;37(4):728-33. DOI: 10.1016/j.clinimag.2012.11.002

38. Sung EK, Nadgir RN, Sakai O. Computed tomographic imaging in head and neck trauma: what the radiologist needs to know. Semin Roentgenol. 2012 Oct;47(4):320-9. DOI: 10.1053/j.ro.2012.05.002

39. Stengel D, Frank M, Matthes G, Schmucker U, Seifert J, Mutze S, Wich M, Hanson B, Giannoudis PV, Ekkernkamp A. Primary pan-computed tomography for blunt multiple trauma: can the whole be better than its parts? Injury. 2009 Nov;40 Suppl 4:S36-46. DOI: 10.1016/j.injury.2009.10.035

40. Dammann F, Bode A, Heuschmid M, Kopp A, Georg C, Pereira PL, Claussen CD. Mehrschicht-Spiral-CT der Nasennebenhöhlen: Erste Erfahrungen unter besonderer Berücksichtigung der Strahlenexposition [Multislice spiral CT of the paranasal sinuses: first experiences using various parameters of radiation dosage]. Rofo. 2000 Aug;172(8):701-6. DOI: 10.1055/s-2000-7175

41. Hoang JK, Eastwood JD, Tebbit CL, Glastonbury CM. Multiplanar sinus CT: a systematic approach to imaging before functional endoscopic sinus surgery. AJR Am J Roentgenol. 2010 Jun;194(6):W527-36. DOI: 10.2214/AJR.09.3584

42. Kröpil P, Cohnen M, Andersen K, Heinen W, Stegmann V, Mödder U. Bildqualität in der Multidetektor-CT der Nasennebenhöhlen: Potenzial zur Dosisreduktion bei Anwendung eines adaptiven Nachverarbeitungsfilters [Image quality in multidetector CT of paranasal sinuses: potential of dose reduction using an adaptive post-processing filter]. Rofo. 2010 Nov;182(11):973-8. DOI: 10.1055/s-0029-1245586

43. Schulz B, Beeres M, Bodelle B, Bauer R, Al-Butmeh F, Thalhammer A, Vogl TJ, Kerl JM. Performance of iterative image reconstruction in CT of the paranasal sinuses: a phantom study. AJNR Am J Neuroradiol. 2013 May;34(5):1072-6. DOI: 10.3174/ajnr.A3339

44. Bulla S, Blanke P, Hassepass F, Krauss T, Winterer JT, Breunig C, Langer M, Pache G. Reducing the radiation dose for low-dose CT of the paranasal sinuses using iterative reconstruction: feasibility and image quality. Eur J Radiol. 2012 Sep;81(9):2246-50. DOI: 10.1016/j.ejrad.2011.05.002

45. Hoxworth JM, Lal D, Fletcher GP, Patel AC, He M, Paden RG, Hara AK. Radiation dose reduction in paranasal sinus CT using model-based iterative reconstruction. AJNR Am J Neuroradiol. 2014 Apr;35(4):644-9. DOI: 10.3174/ajnr.A3749

46. Kastner J, Taudy M, Lisy J, Grabec P, Betka J. Orbital and intracranial complications after acute rhinosinusitis. Rhinology. 2010 Dec;48(4):457-61.

47. Parida PK, Surianarayanan G, Ganeshan S, Saxena SK. Pott's puffy tumor in pediatric age group: a retrospective study. Int J Pediatr Otorhinolaryngol. 2012 Sep;76(9):1274-7. DOI: 10.1016/j.ijporl.2012.05.018

48. Michel M, Jacob S, Roger G, Pelosse B, Laurier D, Le Pointe HD, Bernier MO. Eye lens radiation exposure and repeated head CT scans: A problem to keep in mind. Eur J Radiol. 2012 Aug;81(8):1896-900. DOI: 10.1016/j.ejrad.2011.03.051

49. Shore RE, Neriishi K, Nakashima E. Epidemiological studies of cataract risk at low to moderate radiation doses: (not) seeing is believing. Radiat Res. 2010 Dec;174(6):889-94. DOI: 10.1667/RR1884.1

50. Rehani MM, Vano E, Ciraj-Bjelac O, Kleiman NJ. Radiation and cataract. Radiat Prot Dosimetry. 2011 Sep;147(1-2):300-4. DOI: 10.1093/rpd/ncr299

51. Yuan MK, Tsai DC, Chang SC, Yuan MC, Chang SJ, Chen HW, Leu HB. The risk of cataract associated with repeated head and neck CT studies: a nationwide population-based study. AJR Am J Roentgenol. 2013 Sep;201(3):626-30. DOI: 10.2214/AJR.12.9652

52. Doss M. Conclusion of increased risk of cataracts associated with CT studies of the head may not be justified. AJR Am J Roentgenol. 2014 Apr;202(4):W413. DOI: 10.2214/AJR.13.11867

53. Curtis JR. Computed tomography shielding methods: a literature review. Radiol Technol. 2010 May-Jun;81(5):428-36.

54. Keil B, Wulff J, Schmitt R, Auvanis D, Danova D, Heverhagen JT, Fiebich M, Madsack B, Leppek R, Klose KJ, Zink K. Schutz der Augenlinse in der Computertomografie – Dosisevaluation an einem antropomorphen Phantom mittels Thermolumineszenzdosimetrie und Monte-Carlo-Simulationen [Protection of eye lens in computed tomography – dose evaluation on an anthropomorphic phantom using thermo-luminescent dosimeters and Monte-Carlo simulations]. Rofo. 2008 Dec;180(12):1047-53. DOI: 10.1055/s-2008-1027814

55. Campbell J, Kalra MK, Rizzo S, Maher MM, Shepard JA. Scanning beyond anatomic limits of the thorax in chest CT: findings, radiation dose, and automatic tube current modulation. AJR Am J Roentgenol. 2005 Dec;185(6):1525-30. DOI: 10.2214/AJR.04.1512

56. McCollough CH, Bruesewitz MR, Kofler JM Jr. CT dose reduction and dose management tools: overview of available options. Radiographics. 2006 Mar-Apr;26(2):503-12. DOI: 10.1148/rg.262055138

57. Tack D, De Maertelaer V, Gevenois PA. Dose reduction in multidetector CT using attenuation-based online tube current modulation. AJR Am J Roentgenol. 2003 Aug;181(2):331-4. DOI: 10.2214/ajr.181.2.1810331

58. Wang J, Duan X, Christner JA, Leng S, Grant KL, McCollough CH. Bismuth shielding, organ-based tube current modulation, and global reduction of tube current for dose reduction to the eye at head CT. Radiology. 2012 Jan;262(1):191-8. DOI: 10.1148/radiol.11110470

59. Plessow B, Langner S, Engelhardt J, Hosten N. CT der neuesten Generation - Brauche ich noch einen Strahlenschutz für die Augen. In: 48 Jahrestagung der Deutschen Gesellschaft für Neuroradiologie; 2013 Oct 10-12; Köln, Germany.

60. Muir C, Weiland L. Upper aerodigestive tract cancers. Cancer. 1995 Jan;75(1 Suppl):147-53.

61. Raghavan P, Phillips CD. Magnetic resonance imaging of sinonasal malignancies. Top Magn Reson Imaging. 2007 Aug;18(4):259-67. DOI: 10.1097/RMR.0b013e31815711b7

62. Razek AA, Tawfik AM, Elsorogy LG, Soliman NY. Perfusion CT of head and neck cancer. Eur J Radiol. 2014 Mar;83(3):537-44. DOI: 10.1016/j.ejrad.2013.12.008

63. Razek AA, Huang BY. Soft tissue tumors of the head and neck: imaging-based review of the WHO classification. Radiographics. 2011 Nov-Dec;31(7):1923-54. DOI: 10.1148/rg.317115095

64. Srinivasan A, Mohan S, Mukherji SK. Biologic imaging of head and neck cancer: the present and the future. AJNR Am J Neuroradiol. 2012 Apr;33(4):586-94. DOI: 10.3174/ajnr.A2535

65. Petralia G, Bonello L, Viotti S, Preda L, d'Andrea G, Bellomi M. CT perfusion in oncology: how to do it. Cancer Imaging. 2010;10:8-19.

66. Hoefling NL, McHugh JB, Light E, Kumar B, Walline H, Prince M, Bradford C, Carey TE, Mukherji SK. Human papillomavirus, p16, and epidermal growth factor receptor biomarkers and CT perfusion values in head and neck squamous cell carcinoma. AJNR Am J Neuroradiol. 2013 May;34(5):1062-6, S1-2. DOI: 10.3174/ajnr.A3349

67. Loeffelbein DJ, Souvatzoglou M, Wankerl V, Martinez-Möller A, Dinges J, Schwaiger M, Beer AJ. PET-MRI fusion in head-and-neck oncology: current status and implications for hybrid PET/MRI. J Oral Maxillofac Surg. 2012 Feb;70(2):473-83. DOI: 10.1016/j.joms.2011.02.120

68. Bisdas S, Baghi M, Smolarz A, Pihno NC, Lehnert T, Knecht R, Mack MG, Vogl TJ, Tuerkay S, Koh TS. Quantitative measurements of perfusion and permeability of oropharyngeal and oral cavity cancer, recurrent disease, and associated lymph nodes using first-pass contrast-enhanced computed tomography studies. Invest Radiol. 2007 Mar;42(3):172-9. DOI: 10.1097/01.rli.0000252496.74242.0b

69. Trojanowska A, Trojanowski P, Bisdas S, Staśkiewicz G, Drop A, Klatka J, Bobek-Billewicz B. Squamous cell cancer of hypopharynx and larynx - evaluation of metastatic nodal disease based on computed tomography perfusion studies. Eur J Radiol. 2012 May;81(5):1034-9. DOI: 10.1016/j.ejrad.2011.01.084

70. Bisdas S, Rumboldt Z, Surlan-Popovic K, Baghi M, Koh TS, Vogl TJ, Mack MG. Perfusion CT in squamous cell carcinoma of the upper aerodigestive tract: long-term predictive value of baseline perfusion CT measurements. AJNR Am J Neuroradiol. 2010 Mar;31(3):576-81. DOI: 10.3174/ajnr.A1852

71. Gandhi D, Chepeha DB, Miller T, Carlos RC, Bradford CR, Karamchandani R, Worden F, Eisbruch A, Teknos TN, Wolf GT, Mukherji SK. Correlation between initial and early follow-up CT perfusion parameters with endoscopic tumor response in patients with advanced squamous cell carcinomas of the oropharynx treated with organ-preservation therapy. AJNR Am J Neuroradiol. 2006 Jan;27(1):101-6.

72. Zima AJ, Wesolowski JR, Ibrahim M, Lassig AA, Lassig J, Mukherji SK. Magnetic resonance imaging of oropharyngeal cancer. Top Magn Reson Imaging. 2007 Aug;18(4):237-42. DOI: 10.1097/RMR.0b013e318157112a

73. Hermans R, Meijerink M, Van den Bogaert W, Rijnders A, Weltens C, Lambin P. Tumor perfusion rate determined noninvasively by dynamic computed tomography predicts outcome in head-and-neck cancer after radiotherapy. Int J Radiat Oncol Biol Phys. 2003 Dec;57(5):1351-6.

74. Rumboldt Z, Al-Okaili R, Deveikis JP. Perfusion CT for head and neck tumors: pilot study. AJNR Am J Neuroradiol. 2005 May;26(5):1178-85.

75. Jin G, Su D, Liu L, Zhu X, Xie D, Zhao W. The accuracy of computed tomographic perfusion in detecting recurrent nasopharyngeal carcinoma after radiation therapy. J Comput Assist Tomogr. 2011 Jan-Feb;35(1):26-30. DOI: 10.1097/RCT.0b013e3181f01b93

76. Héran F, Bergès O, Blustajn J, Boucenna M, Charbonneau F, Koskas P, Lafitte F, Nau E, Roux P, Sadik JC, Savatovsky J, Williams M. Tumor pathology of the orbit. Diagn Interv Imaging. 2014 Oct;95(10):933-44. DOI: 10.1016/j.diii.2014.08.002

77. Tailor TD, Gupta D, Dalley RW, Keene CD, Anzai Y. Orbital neoplasms in adults: clinical, radiologic, and pathologic review. Radiographics. 2013 Oct;33(6):1739-58. DOI: 10.1148/rg.336135502

78. de Graaf P, Göricke S, Rodjan F, Galluzzi P, Maeder P, Castelijns JA, Brisse HJ; European Retinoblastoma Imaging Collaboration (ERIC). Guidelines for imaging retinoblastoma: imaging principles and MRI standardization. Pediatr Radiol. 2012 Jan;42(1):2-14. DOI: 10.1007/s00247-011-2201-5

79. Kubal WS. Imaging of orbital trauma. Radiographics. 2008 Oct;28(6):1729-39. DOI: 10.1148/rg.286085523

80. Vogl TJ, Schulz B, Bauer RW, Stöver T, Sader R, Tawfik AM. Dual-energy CT applications in head and neck imaging. AJR Am J Roentgenol. 2012 Nov;199(5 Suppl):S34-9. DOI: 10.2214/AJR.12.9113

81. De Cecco CN, Darnell A, Rengo M, Muscogiuri G, Bellini D, Ayuso C, Laghi A. Dual-energy CT: oncologic applications. AJR Am J Roentgenol. 2012 Nov;199(5 Suppl):S98-S105. DOI: 10.2214/AJR.12.9207

82. Tawfik AM, Kerl JM, Bauer RW, Nour-Eldin NE, Naguib NN, Vogl TJ, Mack MG. Dual-energy CT of head and neck cancer: average weighting of low- and high-voltage acquisitions to improve lesion delineation and image quality-initial clinical experience. Invest Radiol. 2012 May;47(5):306-11. DOI: 10.1097/RLI.0b013e31821e3062

83. Wichmann JL, Kraft J, Nöske EM, Bodelle B, Burck I, Scholtz JE, Frellesen C, Wagenblast J, Kerl JM, Bauer RW, Lehnert T, Vogl TJ, Schulz B. Low-tube-voltage 80-kVp neck CT: evaluation of diagnostic accuracy and interobserver agreement. AJNR Am J Neuroradiol. 2014 Dec;35(12):2376-81. DOI: 10.3174/ajnr.A4052

84. Kapoor V, McCook BM, Torok FS. An introduction to PET-CT imaging. Radiographics. 2004 Mar-Apr;24(2):523-43. DOI: 10.1148/rg.242025724

85. Blodgett TM, Fukui MB, Snyderman CH, Branstetter BF 4th, McCook BM, Townsend DW, Meltzer CC. Combined PET-CT in the head and neck: part 1. Physiologic, altered physiologic, and artifactual FDG uptake. Radiographics. 2005 Jul-Aug;25(4):897-912. DOI: 10.1148/rg.254035156

86. Branstetter BF 4th, Blodgett TM, Zimmer LA, Snyderman CH, Johnson JT, Raman S, Meltzer CC. Head and neck malignancy: is PET/CT more accurate than PET or CT alone? Radiology. 2005 May;235(2):580-6. DOI: 10.1148/radiol.2352040134

87. Dizendorf EV, Baumert BG, von Schulthess GK, Lütolf UM, Steinert HC. Impact of whole-body 18F-FDG PET on staging and managing patients for radiation therapy. J Nucl Med. 2003 Jan;44(1):24-9.

88. Farber LA, Benard F, Machtay M, Smith RJ, Weber RS, Weinstein GS, Chalian AA, Alavi A, Rosenthal DI. Detection of recurrent head and neck squamous cell carcinomas after radiation therapy with 2-18F-fluoro-2-deoxy-D-glucose positron emission tomography. Laryngoscope. 1999 Jun;109(6):970-5.

89. Fukui MB, Blodgett TM, Snyderman CH, Johnson JJ, Myers EN, Townsend DW, Meltzer CC. Combined PET-CT in the head and neck: part 2. Diagnostic uses and pitfalls of oncologic imaging. Radiographics. 2005 Jul-Aug;25(4):913-30. DOI: 10.1148/rg.254045136

90. Laubenbacher C, Saumweber D, Wagner-Manslau C, Kau RJ, Herz M, Avril N, Ziegler S, Kruschke C, Arnold W, Schwaiger M. Comparison of fluorine-18-fluorodeoxyglucose PET, MRI and endoscopy for staging head and neck squamous-cell carcinomas. J Nucl Med. 1995 Oct;36(10):1747-57.

91. Wong WL, Chevretton EB, McGurk M, Hussain K, Davis J, Beaney R, Baddeley H, Tierney P, Maisey M. A prospective study of PET-FDG imaging for the assessment of head and neck squamous cell carcinoma. Clin Otolaryngol Allied Sci. 1997 Jun;22(3):209-14.

92. Hanamoto A, Tatsumi M, Takenaka Y, Hamasaki T, Yasui T, Nakahara S, Yamamoto Y, Seo Y, Isohashi F, Ogawa K, Hatazawa J, Inohara H. Volumetric PET/CT parameters predict local response of head and neck squamous cell carcinoma to chemoradiotherapy. Cancer Med. 2014 Oct;3(5):1368-76. DOI: 10.1002/cam4.295

93. Purohit BS, Ailianou A, Dulguerov N, Becker CD, Ratib O, Becker M. FDG-PET/CT pitfalls in oncological head and neck imaging. Insights Imaging. 2014 Oct;5(5):585-602. DOI: 10.1007/s13244-014-0349-x

94. Rangaswamy B, Fardanesh MR, Genden EM, Park EE, Fatterpekar G, Patel Z, Kim J, Som PM, Kostakoglu L. Improvement in the detection of locoregional recurrence in head and neck malignancies: F-18 fluorodeoxyglucose-positron emission tomography/computed tomography compared to high-resolution contrast-enhanced computed tomography and endoscopic examination. Laryngoscope. 2013 Nov;123(11):2664-9. DOI: 10.1002/lary.24077

95. Dunsky KA, Wehrmann DJ, Osman MM, Thornberry BM, Varvares MA. PET-CT and the detection of the asymptomatic recurrence or second primary lesions in the treated head and neck cancer patient. Laryngoscope. 2013 Sep;123(9):2161-4. DOI: 10.1002/lary.23941

96. Kim JW, Roh JL, Kim JS, Lee JH, Cho KJ, Choi SH, Nam SY, Kim SY. (18)F-FDG PET/CT surveillance at 3-6 and 12 months for detection of recurrence and second primary cancer in patients with head and neck squamous cell carcinoma. Br J Cancer. 2013 Dec;109(12):2973-9. DOI: 10.1038/bjc.2013.668

97. Roh JL, Park JP, Kim JS, Lee JH, Cho KJ, Choi SH, Nam SY, Kim SY. 18F fluorodeoxyglucose PET/CT in head and neck squamous cell carcinoma with negative neck palpation findings: a prospective study. Radiology. 2014 Apr;271(1):153-61. DOI: 10.1148/radiol.13131470

98. Subramaniam RM, Truong M, Peller P, Sakai O, Mercier G. Fluorodeoxyglucose-positron-emission tomography imaging of head and neck squamous cell cancer. AJNR Am J Neuroradiol. 2010 Apr;31(4):598-604. DOI: 10.3174/ajnr.A1760

99. Marcus C, Ciarallo A, Tahari AK, Mena E, Koch W, Wahl RL, Kiess AP, Kang H, Subramaniam RM. Head and neck PET/CT: therapy response interpretation criteria (Hopkins Criteria)-interreader reliability, accuracy, and survival outcomes. J Nucl Med. 2014 Sep;55(9):1411-6. DOI: 10.2967/jnumed.113.136796

100. Kapoor V, Fukui MB, McCook BM. Role of 18FFDG PET/CT in the treatment of head and neck cancers: posttherapy evaluation and pitfalls. AJR Am J Roentgenol. 2005 Feb;184(2):589-97. DOI: 10.2214/ajr.184.2.01840589

101. Porceddu SV, Jarmolowski E, Hicks RJ, Ware R, Weih L, Rischin D, Corry J, Peters LJ. Utility of positron emission tomography for the detection of disease in residual neck nodes after (chemo)radiotherapy in head and neck cancer. Head Neck. 2005 Mar;27(3):175-81. DOI: 10.1002/hed.20130

102. Schöder H, Fury M, Lee N, Kraus D. PET monitoring of therapy response in head and neck squamous cell carcinoma. J Nucl Med. 2009 May;50 Suppl 1:74S-88S. DOI: 10.2967/jnumed.108.057208

103. Chen SW, Hsieh TC, Yen KY, Yang SN, Wang YC, Chien CR, Liang JA, Kao CH. Interim FDG PET/CT for predicting the outcome in patients with head and neck cancer. Laryngoscope. 2014 Dec;124(12):2732-8. DOI: 10.1002/lary.24826

104. Joo YH, Yoo IeR, Cho KJ, Park JO, Nam IC, Kim CS, Kim MS. Relationship between extracapsular spread and FDG PET/CT in oropharyngeal squamous cell carcinoma. Acta Otolaryngol. 2013 Oct;133(10):1073-9. DOI: 10.3109/00016489.2013.799292

105. Joo YH, Yoo IR, Cho KJ, Park JO, Nam IC, Kim CS, Kim SY, Kim MS. The value of preoperative 18F-FDG PET/CT for the assessing contralateral neck in head and neck cancer patients with unilateral node metastasis (N1-3). Clin Otolaryngol. 2014 Dec;39(6):338-44. DOI: 10.1111/coa.12295

106. Paes FM, Singer AD, Checkver AN, Palmquist RA, De La Vega G, Sidani C. Perineural spread in head and neck malignancies: clinical significance and evaluation with 18F-FDG PET/CT. Radiographics. 2013 Oct;33(6):1717-36. DOI: 10.1148/rg.336135501

107. Abdel Razek AA, Kandeel AY, Soliman N, El-shenshawy HM, Kamel Y, Nada N, Denewar A. Role of diffusion-weighted echo-planar MR imaging in differentiation of residual or recurrent head and neck tumors and posttreatment changes. AJNR Am J Neuroradiol. 2007 Jun-Jul;28(6):1146-52. DOI: 10.3174/ajnr.A0491

108. Langner S, Krueger PC, Lindner T, Niendorf T, Stachs O. In-vivo-Magnetresonanzmikroskopie des humanen Auges [In vivo MR microscopy of the human eye]. Klin Monbl Augenheilkd. 2014 Oct;231(10):1016-22. DOI: 10.1055/s-0034-1368575

109. Casselman JW. The skull base: tumoral lesions. Eur Radiol. 2005 Mar;15(3):534-42. DOI: 10.1007/s00330-004-2532-9

110. Som PM, Shapiro MD, Biller HF, Sasaki C, Lawson W. Sinonasal tumors and inflammatory tissues: differentiation with MR imaging. Radiology. 1988 Jun;167(3):803-8. DOI: 10.1148/radiology.167.3.3363145

111. Madani G, Beale TJ, Lund VJ. Imaging of sinonasal tumors. Semin Ultrasound CT MR. 2009 Feb;30(1):25-38.

112. Schaefer PW, Grant PE, Gonzalez RG. Diffusion-weighted MR imaging of the brain. Radiology. 2000 Nov;217(2):331-45. DOI: 10.1148/radiology.217.2.r00nv24331

113. Sumi M, Ichikawa Y, Nakamura T. Diagnostic ability of apparent diffusion coefficients for lymphomas and carcinomas in the pharynx. Eur Radiol. 2007 Oct;17(10):2631-7. DOI: 10.1007/s00330-007-0588-z

114. Sasaki M, Eida S, Sumi M, Nakamura T. Apparent diffusion coefficient mapping for sinonasal diseases: differentiation of benign and malignant lesions. AJNR Am J Neuroradiol. 2011 Jun-Jul;32(6):1100-6. DOI: 10.3174/ajnr.A2434

115. Vandecaveye V, De Keyzer F, Vander Poorten V, Dirix P, Verbeken E, Nuyts S, Hermans R. Head and neck squamous cell carcinoma: value of diffusion-weighted MR imaging for nodal staging. Radiology. 2009 Apr;251(1):134-46. DOI: 10.1148/radiol.2511080128

116. Barchetti F, Pranno N, Giraldi G, Sartori A, Gigli S, Barchetti G, Lo Mele L, Marsella LT. The role of 3 Tesla diffusion-weighted imaging in the differential diagnosis of benign versus malignant cervical lymph nodes in patients with head and neck squamous cell carcinoma. Biomed Res Int. 2014;2014:532095. DOI: 10.1155/2014/532095

117. Mahalingappa YB, Khalil HS. Sinonasal malignancy: presentation and outcomes. J Laryngol Otol. 2014 Jul;128(7):654-7. DOI: 10.1017/S0022215114001066

118. Dubrulle F, Souillard R, Hermans R. Extension patterns of nasopharyngeal carcinoma. Eur Radiol. 2007 Oct;17(10):2622-30. DOI: 10.1007/s00330-007-0616-z

119. Eisen MD, Yousem DM, Montone KT, Kotapka MJ, Bigelow DC, Bilker WB, Loevner LA. Use of preoperative MR to predict dural, perineural, and venous sinus invasion of skull base tumors. AJNR Am J Neuroradiol. 1996 Nov-Dec;17(10):1937-45.

120. Eisen MD, Yousem DM, Loevner LA, Thaler ER, Bilker WB, Goldberg AN. Preoperative imaging to predict orbital invasion by tumor. Head Neck. 2000 Aug;22(5):456-62. DOI: 10.1002/1097-0347(200008)22:5<456::AID-HED3>3.0.CO;2-N

121. Loevner LA, Sonners AI. Imaging of neoplasms of the paranasal sinuses. Magn Reson Imaging Clin N Am. 2002 Aug;10(3):467-93. DOI: 10.1016/S1064-9689(02)00006-5

122. Yousem DM, Gad K, Tufano RP. Resectability issues with head and neck cancer. AJNR Am J Neuroradiol. 2006 Nov-Dec;27(10):2024-36.

123. Ginsberg LE. MR imaging of perineural tumor spread. Neuroimaging Clin N Am. 2004 Nov;14(4):663-77.

124. Lambrecht M, Van Calster B, Vandecaveye V, De Keyzer F, Roebben I, Hermans R, Nuyts S. Integrating pretreatment diffusion weighted MRI into a multivariable prognostic model for head and neck squamous cell carcinoma. Radiother Oncol. 2014 Mar;110(3):429-34. DOI: 10.1016/j.radonc.2014.01.004

125. Nakajo M, Nakajo M, Kajiya Y, Tani A, Kamiyama T, Yonekura R, Fukukura Y, Matsuzaki T, Nishimoto K, Nomoto M, Koriyama C. FDG PET/CT and diffusion-weighted imaging of head and neck squamous cell carcinoma: comparison of prognostic significance between primary tumor standardized uptake value and apparent diffusion coefficient. Clin Nucl Med. 2012 May;37(5):475-80. DOI: 10.1097/RLU.0b013e318248524a

126. Sepahdari AR, Politi LS, Aakalu VK, Kim HJ, Razek AA. Diffusion-weighted imaging of orbital masses: multi-institutional data support a 2-ADC threshold model to categorize lesions as benign, malignant, or indeterminate. AJNR Am J Neuroradiol. 2014 Jan;35(1):170-5. DOI: 10.3174/ajnr.A3619

127. Fatima Z, Ichikawa T, Ishigame K, Motosugi U, Waqar AB, Hori M, Iijima H, Araki T. Orbital masses: the usefulness of diffusion-weighted imaging in lesion categorization. Clin Neuroradiol. 2014 Jun;24(2):129-34. DOI: 10.1007/s00062-013-0234-x

128. Sepahdari AR, Aakalu VK, Kapur R, Michals EA, Saran N, French A, Mafee MF. MRI of orbital cellulitis and orbital abscess: the role of diffusion-weighted imaging. AJR Am J Roentgenol. 2009 Sep;193(3):W244-50. DOI: 10.2214/AJR.08.1838

129. Politi LS, Godi C, Cammarata G, Ambrosi A, Iadanza A, Lanzi R, Falini A, Bianchi Marzoli S. Magnetic resonance imaging with diffusion-weighted imaging in the evaluation of thyroid-associated orbitopathy: getting below the tip of the iceberg. Eur Radiol. 2014 May;24(5):1118-26. DOI: 10.1007/s00330-014-3103-3

130. Erb-Eigner K, Willerding G, Taupitz M, Hamm B, Asbach P. Diffusion-weighted imaging of ocular melanoma. Invest Radiol. 2013 Oct;48(10):702-7. DOI: 10.1097/RLI.0b013e31828eea67

131. Porter DA, Heidemann RM. High resolution diffusion-weighted imaging using readout-segmented echo-planar imaging, parallel imaging and a two-dimensional navigator-based reacquisition. Magn Reson Med. 2009 Aug;62(2):468-75. DOI: 10.1002/mrm.22024

132. Espinoza S, Malinvaud D, Siauve N, Halimi P. Perfusion in ENT imaging. Diagn Interv Imaging. 2013 Dec;94(12):1225-40. DOI: 10.1016/j.diii.2013.06.003

133. Bernstein JM, Homer JJ, West CM. Dynamic contrast-enhanced magnetic resonance imaging biomarkers in head and neck cancer: potential to guide treatment? A systematic review. Oral Oncol. 2014 Oct;50(10):963-70. DOI: 10.1016/j.oraloncology.2014.07.011

134. Lee SJ, Seo HJ, Cheon GJ, Kim JH, Kim EE, Kang KW, Paeng JC, Chung JK, Lee DS. Usefulness of Integrated PET/MRI in Head and Neck Cancer: A Preliminary Study. Nucl Med Mol Imaging. 2014 Jun;48(2):98-105. DOI: 10.1007/s13139-013-0252-2

135. Becker M, Zaidi H. Imaging in head and neck squamous cell carcinoma: the potential role of PET/MRI. Br J Radiol. 2014 Apr;87(1036):20130677. DOI: 10.1259/bjr.20130677

136. Kuhn FP, Hüllner M, Mader CE, Kastrinidis N, Huber GF, von Schulthess GK, Kollias S, Veit-Haibach P. Contrast-enhanced PET/MR imaging versus contrast-enhanced PET/CT in head and neck cancer: how much MR information is needed? J Nucl Med. 2014 Apr;55(4):551-8. DOI: 10.2967/jnumed.113.125443

137. Queiroz MA, Hüllner M, Kuhn F, Huber G, Meerwein C, Kollias S, von Schulthess G, Veit-Haibach P. PET/MRI and PET/CT in follow-up of head and neck cancer patients. Eur J Nucl Med Mol Imaging. 2014 Jun;41(6):1066-75. DOI: 10.1007/s00259-014-2707-9

138. Partovi S, Kohan A, Vercher-Conejero JL, Rubbert C, Margevicius S, Schluchter MD, Gaeta C, Faulhaber P, Robbin MR. Qualitative and quantitative performance of 18F-FDG-PET/MRI versus 18F-FDG-PET/CT in patients with head and neck cancer. AJNR Am J Neuroradiol. 2014 Oct;35(10):1970-5. DOI: 10.3174/ajnr.A3993

139. Queiroz MA, Hüllner M, Kuhn F, Huber G, Meerwein C, Kollias S, von Schulthess G, Veit-Haibach P. Use of diffusion-weighted imaging (DWI) in PET/MRI for head and neck cancer evaluation. Eur J Nucl Med Mol Imaging. 2014 Dec;41(12):2212-21. DOI: 10.1007/s00259-014-2867-7

140. Lodder WL, Vogel WV, Lange CA, Hamming-Vrieze O, Van Velthuysen ML, Pameijer FA, Balm AJ, Van Den Brekel MW. Detection of extranodal spread in head and neck cancer with [18F]FDG PET and MRI: improved accuracy? Q J Nucl Med Mol Imaging. 2015 Sep;59(3):327-35.

## Corresponding author:

Sönke Langner, MD, PhD
Institute for Diagnostic Radiology and Neuroradiology, University Medicine Greifswald, Ferdinand-Sauerbruch-Str. 1, 17475 Greifswald, Germany, Phone: + 49 3834-86-6960, Fax: + 49-3834-86-7097
soenke.Langner@uni-Greifswald.de